

## 13.1 General Aspects

### 13.1.1 Thermal Lensing in Solid State Lasers

In solid state lasers the active medium exhibits the properties of a thermally induced lens when the material is pumped. The refractive power is brought about by a combination of heat generation due to absorption of pump and laser radiation and the flow of heat to the outer periphery due to cooling. For a laser rod this leads to a temperature distribution which is parabolic with respect to the radial position  $r$  if the thermal conductivity is constant and the medium is illuminated homogeneously by the excitation source (Fig. 13.1). This results in a similar radial dependence of the index of refraction, neglecting polarization effects:

$$n(r) = n_0 (1 - \gamma r^2) \quad (13.1)$$

where  $n_0$  is the index of refraction at the center. A bundle of parallel rays incident on the laser rod is focused by the thermal lens for  $\gamma > 0$  since the optical path length  $n(r)l$  inside the medium is longer for rays being closer to the center of the rod.

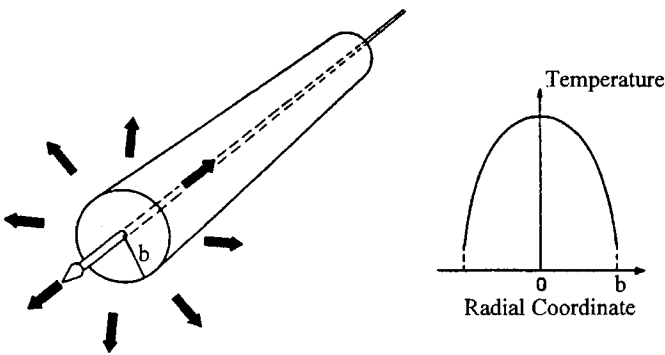


**Fig. 13.1** Heat deposition by the pump process and cooling of the outer periphery generates a parabolic temperature profile in solid state laser rods.

This is in contrast to common lenses where the change in the optical path length is generated by an increased thickness at the center of the lens and not by an increase in the index of refraction. To a first approximation, the refractive power  $D$  of a rod of length  $\ell$  is given by:

$$D = 2\gamma n_0 \ell \quad (13.2)$$

whereby effects caused by the bending of the rod endfaces are neglected [4.2,4.83, 4.84,4.89]. The proportionality of the parameter  $\gamma$  to the dissipated heat  $P_H$  leads to a linear relationship between the pump power and the refractive power. For a rod with radius  $b$ , one gets for the averaged value (radial/azimuthal polarization):

$$D = \frac{1}{K 2\pi b^2} \left[ \frac{dn}{dT} + \epsilon \right] P_H = \frac{1}{K 2\pi b^2} \left[ \frac{dn}{dT} + \epsilon \right] \chi \eta_{excit} P_{pump} \quad (13.3)$$

with:

$K$	:	thermal conductivity
$dn/dT$	:	temperature derivative of the index of refraction
$\epsilon$	:	stress dependent variation of the refractive index
$\chi$	:	thermal load parameter
$\eta_{excit}$	:	excitation efficiency (see Sec. 9.3)
$P_{pump}$	:	electrical pump power for flashlamp pumping and optical pump power for diode pumping

The thermal load parameter  $\chi$  is the ratio of the heat  $P_H$  to the power  $P_{UL}$  available in the form of population inversion. For flashlamp pumped Nd:YAG rods in pulsed and cw operation the thermal load parameter typically is between 2-3 and 1-1.5, respectively, depending on the excitation spectrum. For diode pumping at 808nm, the thermal load parameter is about 0.33. The stress dependent parameter  $\epsilon$  accounts for the variations in refractive power between radial and azimuthal polarization; in Nd:YAG the refractive power for radial polarized light is about 15% higher than the refractive power for azimuthally polarized light. The material constants in (13.3) can be combined in a constant  $C$  with:

$$D = \frac{C}{A} \chi \eta_{excit} P_{pump} \quad (13.4)$$

We see that the thermal lens does not depend on the length of the active medium and that it is inversely proportional to the cross sectional area  $A = \pi b^2$  of the rod material. The constant  $C$  is a characteristic of the laser material. This expression is usually simplified by introducing the thermal lensing coefficient  $\alpha = C\chi\eta_{excit}$ :

$$D = \frac{\alpha}{A} P_{pump} \quad (13.5)$$

Table 13.1 gives an overview of typical thermal lensing coefficients for flashlamp pumped solid state rods and the corresponding refractive powers for a rod diameter of 10mm. For diode pumping, the thermal lensing coefficient is about 30% lower ( $P_{pump}$  is the optical pump power absorbed by the laser material). Thermal lensing coefficients for diode-pumped materials are given in Table 13.2. Measured thermal lensing coefficients for end-pumped Vanadate are depicted in Fig.13.2.

**Table 13.1** Thermal lensing coefficients of flashlamp pumped solid state laser rods and the corresponding refractive powers at 1kW of electrical pump power for a rod diameter of 10mm. The range of the thermal lensing coefficient is generated by different pump conditions (efficiency!) and variations in crystal quality.

Material	$\alpha$ [ $\mu\text{m}/\text{kW}$ ]	$D[\text{m}^{-1}]$
Nd:YAG (1064nm)	21 - 30	0.27 - 0.38
Nd:glass (1050nm)	150 -190	1.91 - 2.42
Nd:Cr:GSGG (1064nm)	37 - 57	0.47 - 0.73
Nd:Cr:GGG (1064nm)	75 - 95	0.95 - 1.21
Nd:YAP (1058nm)	37 - 69	0.47 - 0.88
Nd:YLF (1053nm, 1047nm)	-3*; 14**	- 0.048; 0.018
Alexandrite (760nm)	7 - 12	0.09 - 0.15

\*  $\sigma$ -polarized at  $\lambda=1053\text{nm}$     \*\* $\pi$ -polarized at  $\lambda=1047\text{nm}$

**Table 13.2** Thermal lensing coefficients of optically pumped solid state laser rods and the corresponding refractive powers at 100W of absorbed optical pump power for a rod diameter of 3mm. The range of the thermal lensing coefficient is caused by differences in pumping geometry and doping concentration. In end-pumped lasers, a lower doping concentration results in a lower thermal lensing coefficient due to lower temperatures and less pronounced bulging of the end face. For low doping concentrations (<0.4% for Nd:YAG, and < 0.25% in Nd:YVO<sub>4</sub>), the lower value of the thermal lensing coefficient applies. A flat-top transverse pump profile is assumed. For a Gaussian pump profile, the thermal lensing coefficient is two times higher than the values shown.

Material	pump wavelength [nm]	$\alpha$ [ $\mu\text{m}/\text{W}$ ]	$D[\text{m}^{-1}]$
Nd:YAG (1064nm)	808	0.10 - 0.15	1.41- 2.12
Nd:glass (1054nm)	808	0.70 - 1.0	9.9 - 14.1
Nd:YVO <sub>4</sub> (1064nm)	808	0.09 - 0.14	1.27 - 1.98
Nd:YVO <sub>4</sub> (1064nm)	879	0.06 - 0.10	0.85 - 1.41
Nd:GdVO <sub>4</sub> (1064nm)	808	0.11 - 0.15	1.55 - 2.12
Nd:YAP (1079nm)	795	0.18 - 0.26	2.55 - 3.67
Nd:YLF (1053nm, 1047nm)	806	-0.015*; 0.07**	- 0.21 ; 0.99
Yb:YAG	940	0.04 - 0.07	0.56 - 0.99
Ti:sapphire	532	0.07 - 0.12	0.99 - 1.7

\*  $\sigma$ -polarized at  $\lambda=1053\text{nm}$     \*\* $\pi$ -polarized at  $\lambda=1047\text{nm}$

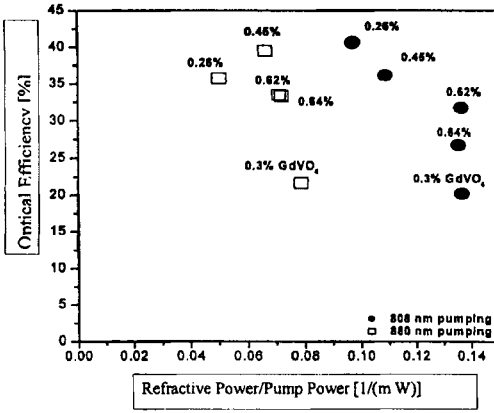


Fig. 13.2 Measured optical efficiencies and refractive powers  $D$  for end-pumped Nd:YVO<sub>4</sub> lasers at different pump diode wavelengths and a pump power of 18W (flat-top transverse pump distribution). Parameter is the doping concentration. Measurements for GdVO<sub>4</sub> are also shown. Pump spot diameter: 1.1mm [4.122] (© OSA 2002).

Since the lens becomes stronger as the thermal load is increased, the beam propagation inside and outside the resonator will become dependent on the pump power. Therefore, the beam quality and the focusing characteristics of the laser beam change with the laser output power. Thermal lensing is the dominant effect for beam quality and power limitations in solid state lasers. However, thermal lensing also occurs in gas lasers [4.86], but compared to solid state lasers, the focal lengths are two orders of magnitude longer.

### 13.1.2 Ray Transfer Matrices

Similar to the previous discussion of optical resonators, the theoretical description of resonators with an internal variable lens is based on ray transfer matrices. For a thermal lens with an index of refraction given by (13.1) the ray transfer matrix reads [4.103]:

$$M_{TL} = \begin{pmatrix} \cos(\sqrt{2\gamma}\ell) & \frac{1}{\sqrt{2\gamma}n_0}\sin(\sqrt{2\gamma}\ell) \\ -\sqrt{2\gamma}n_0\sin(\sqrt{2\gamma}\ell) & \cos(\sqrt{2\gamma}\ell) \end{pmatrix} \tag{13.6}$$

In general, the relation  $\sqrt{2\gamma}\ell \ll 1$  holds and the ray transfer matrix can be simplified by expanding the matrix elements into series of linear and quadratic terms:

$$M_{TL} = \begin{pmatrix} 1 - Dh & \ell/n_0 \\ -D & 1 - Dh \end{pmatrix} \tag{13.7}$$

with:  $D = 2\gamma n_0 \ell$  and  $h = \ell/(2n_0)$

Thus, we get the ray transfer matrix of a thick lens with refractive power  $D$  with the principal planes being located inside the rod at a distance  $h$  from the endfaces. The ray transfer matrix of a thick lens can be used for  $\sqrt{Dl/n_0} < 0.5$ . At the upper limit, the difference in beam radii and beam propagation are on the order of one percent compared to the correct ray transfer matrix (13.6). For a 100 mm long Nd:YAG rod ( $n_0=1.82$ ), that means that the refractive power can be as high as 4.5 Diopters before the matrix (13.6) has to be used to calculate the ray propagation. This approximation is usually valid for all solid state lasers so that the ray transfer matrix of the thick lens is used from now on.

In Sec. 8.1, resonators with an internal thin lens were already discussed. All results derived in this section are still valid with the exception that  $d_1$  and  $d_2$  now represent the distances of the principal planes to the mirrors [4.80,4.81,4.93,4.100]. In order to determine the propagation of the Gaussian beam (fundamental mode) inside the resonator, the concept of the equivalent g-parameters is applied. An optical resonator with an internal thermal lens (lens resonator) exhibits the same Gaussian beam radii at the mirrors as the equivalent empty resonator with the equivalent g-parameters  $g_i^*$  and the equivalent resonator length  $L^*$  with (Fig. 13.3):

$$g_i^* = g_i - Dd_j(1 - d_j/\rho_i) \quad ij=1,2; i \neq j \quad (13.8)$$

$$g_i = 1 - (d_1 + d_2)/\rho_i \quad (13.9)$$

$$L^* = d_1 + d_2 - Dd_1d_2 \quad (13.10)$$

Note that the term  $d_1+d_2$  is the effective resonator length  $L_{eff}$  of the resonator (see Sec. 9.2) which means that we could replace the thick lens by a thin lens with  $d_1, d_2$  being the distances to the two mirrors. The resulting ray transfer matrix for a transit between the mirrors would be identical. By using the equivalent resonator parameters, the Gaussian beam propagation inside the resonator can be calculated by making use of the fact that the mirror surfaces are surfaces of constant phase for the beam.

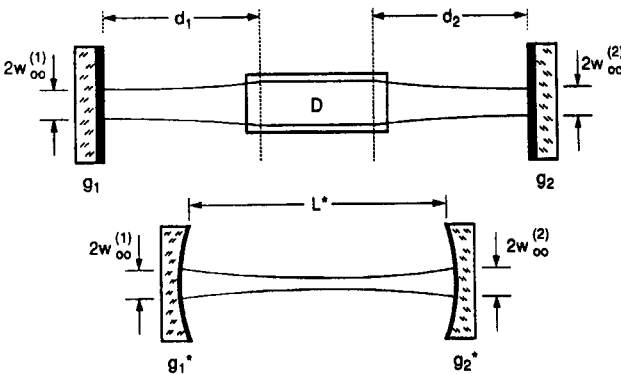


Fig. 13.3 The lens resonator and its equivalent resonator. Both resonators exhibit identical Gaussian beam radii at the mirrors but the beam propagation is different.

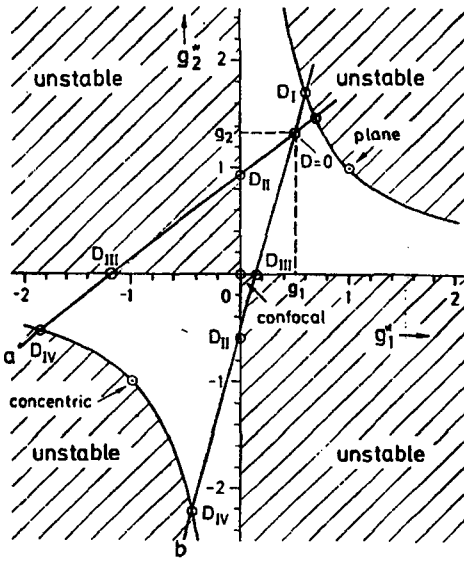


Fig. 13.4 Lens resonators with one internal lens move along straight lines through the equivalent  $g$ -diagram as the refractive power  $D$  is increased. The slope of the lines depends on the position of the medium and on the mirror curvatures.

The properties of a lens resonator can be visualized in the equivalent  $g$ -diagram (Fig. 13.4). The resonator starts at the point  $(g_1, g_2)$  and moves along a straight line through the diagram with increasing refractive power. In general, the lens resonator passes through stable zones and unstable zones. A lens resonator is called stable for  $0 < g_1^* g_2^* < 1$  and unstable for  $|g_1^* g_2^*| > 1$ . Four characteristic refractive powers exist at which the resonator intersects stability limits (see Fig. 13.4):

$$a) \ g_1^* g_2^* = 1 \text{ and } g_1^* > 0 : \quad D_I = - \frac{1}{\rho_1 - d_1} - \frac{1}{\rho_2 - d_2} \quad (13.11)$$

$$b) \ g_1^* = 0 : \quad D_{II} = - \frac{1}{\rho_1 - d_1} + \frac{1}{d_2} \quad (13.12)$$

$$c) \ g_2^* = 0 : \quad D_{III} = \frac{1}{d_1} - \frac{1}{\rho_2 - d_2} \quad (13.13)$$

$$d) \ g_1^* g_2^* = 1 \text{ and } g_1^* < 0 : \quad D_{IV} = \frac{1}{d_1} + \frac{1}{d_2} \quad (13.14)$$

If  $|D_{II}| < |D_{III}|$  holds, the lens resonator passes through the upper left unstable region in Fig. 13.4. Resonators with the property  $D_{II} = D_{III}$  can reach the origin of the diagram (confocal resonator). These resonators are characterized by the condition:

$$\frac{d_2}{d_1} = \sqrt{\frac{g_1}{g_2}} \tag{13.15}$$

which for a resonator with two identical mirrors means that the lens is located in the center.

**Example:**

Nd:YAG rod,  $l=150\text{mm}$ ,  $n_0=1.82$ ; resonator :  $\rho_1=\infty$ ,  $\rho_2=3\text{m}$ ,  $d_1=0.3\text{m}$ ,  $d_2=0.5\text{m}$

The distance of the mirrors from the rod endfaces are 0.259m and 0.459m which means that the geometrical resonator length is 0.868m. The resonator starts at the point  $g_1=1$ ,  $g_2=0.733$  in the equivalent g-diagram. The four characteristic refractive powers are:

$$D_I = -0.4\text{m}^{-1}, D_{II} = 2.0\text{m}^{-1}, D_{III} = 2.933\text{m}^{-1}, D_{IV} = 5.333\text{m}^{-1}$$

## 13.2 Stable Resonators

### 13.2.1 Fundamental Mode Operation

By using the equivalent resonator parameters, the beam propagation of the Gaussian beam with wavelength  $\lambda$  inside the lens resonator can be derived from the known beam radii at the resonator mirrors. The Gaussian beam exhibits two waists whose position and radius are a function of the refractive power. The following relations hold for the resonator shown in Fig. 13.5:

Beam radius at mirror  $i$  :  $w_i^2 = \frac{\lambda L^*}{\pi} \sqrt{\frac{g_j^*}{g_i^*(1-g_1^*g_2^*)}}$  (13.16)

Waist radii :  $w_{0i}^2 = \frac{\lambda L^*}{\pi} \frac{\sqrt{g_i^*g_2^*(1-g_1^*g_2^*)}}{g_j^*(L^*/\rho_j)^2 + g_i^*(1-g_1^*g_2^*)}$  (13.17)

Beam radius at the principal planes of the thermal lens:

$$w_L^2 = w_1^2 \left[ \left(1 - \frac{d_1}{\rho_1}\right)^2 + \left(\frac{d_1}{L^*}\right)^2 \frac{g_1^*(1-g_1^*g_2^*)}{g_2^*} \right] \tag{13.18}$$

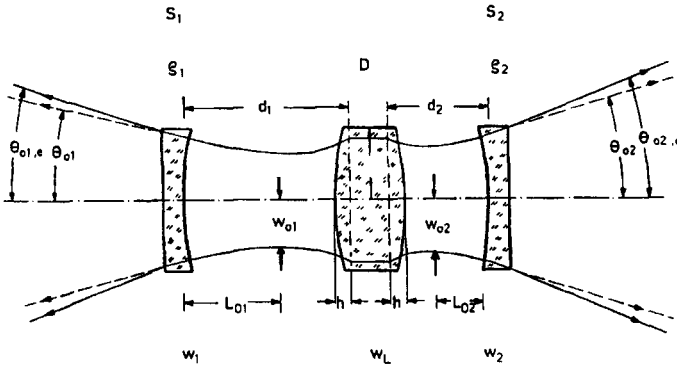


Fig. 13.5 Propagation of the Gaussian beam in a lens resonator.

Location of beam waist  $i$  : 
$$L_{0i} = L \frac{g_j^* L^* / \rho_i}{g_j^* (L^* / \rho_i)^2 + g_i^* (1 - g_1^* g_2^*)} \quad (13.19)$$

Half angle of divergence : 
$$\theta_{0i} = \frac{\lambda}{\pi w_{0i}} \quad (13.20)$$

The beam waist  $i$  is located to the left of mirror  $i$  for  $L_{0i} < 0$  and to the right for  $L_{0i} > 0$ . In Fig. 13.5,  $L_{01}$  is positive and  $L_{02}$  is negative. Due to the thermal lens, the two angles of divergence are different because the two waist radii are not equal. The beam parameter product is the same on both sides of the resonator and is given by:

$$w_{01} \theta_{01} = w_{02} \theta_{02} = \frac{\lambda}{\pi} \quad (13.21)$$

Unfortunately, the above shown expressions are too complicated to discuss in general; therefore, it is necessary to calculate the beam parameters to get a feeling for the beam characteristics. In the following we present the dependence of the beam radii and the angle of divergence on the refractive power for the resonator discussed in the previous example. The Gaussian beam is an eigensolution for this resonator if the refractive power lies within the ranges  $0\text{m}^{-1}$ - $2\text{m}^{-1}$  and  $2.93\text{m}^{-1}$ - $5.33\text{m}^{-1}$ . Outside the stable zones, real values are not provided by (13.16)-(13.20). Figure 13.6 presents the beam radius in the medium  $w_L$ , the waist radii  $w_{0i}$ , and the half angles of divergence  $\theta_{0i}$  as a function of the refractive power. The stability limits are characterized by infinite or zero waist radii whereby the divergence exhibits a reciprocal behavior since the beam parameter product has to remain constant.

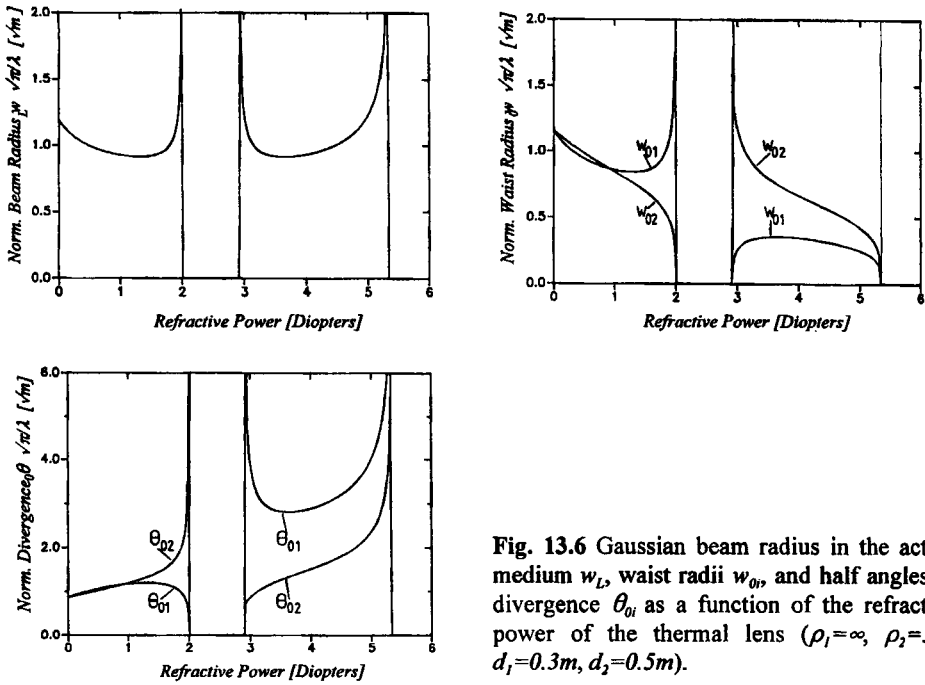


**Fig. 13.6** Gaussian beam radius in the active medium  $w_L$ , waist radii  $w_{0i}$ , and half angles of divergence  $\theta_{0i}$  as a function of the refractive power of the thermal lens ( $\rho_1 = \infty$ ,  $\rho_2 = 3\text{m}$ ,  $d_1 = 0.3\text{m}$ ,  $d_2 = 0.5\text{m}$ ).

Typically, the Gaussian beam radius inside the medium exhibits a minimum which is approximately located in the middle of each stable zone. If  $\Delta D$  denotes the range of the refractive power within which the resonator is stable, the minimum Gaussian beam radius in the medium reads:

$$w_{L,\min}^2 = \frac{4\lambda}{k \pi \Delta D} \tag{13.22}$$

with  $k = 1$  if the confocal point  $g_1^* = g_2^* = 0$  is passed and  $k = 2$  elsewhere.

For the resonator in Fig. 13.6 and a wavelength of  $\lambda = 1.064\mu\text{m}$ , we get a minimum beam radius of  $0.531\text{mm}$  in both stable zones. The Gaussian beam radius in the medium stays relatively constant over a range of the refractive power that covers about 90% of the stable zone. Within this range fundamental mode operation can be attained if an aperture is placed in front of the medium whereby the aperture radius  $a$  needs to be adapted to the Gaussian beam radius:

$$a = 1.3 w_{L,\min} \tag{13.23}$$

### 13.2.2 Transverse Multimode Operation

If no aperture is used inside the resonator, higher order transverse modes will oscillate whose beam radii are smaller than the radius  $b$  of the active medium. The number of oscillating modes is equivalent to the beam quality factor  $M^2$  and can, to a good approximation, be calculated with:

$$M^2 = \left( \frac{b}{w_L} \right)^2 \quad (13.24)$$

where  $w_L$  is the Gaussian beam radius at the principal planes of the thermal lens. Since the Gaussian beam radius changes with increasing thermal lens power, the beam quality of multimode lasers is a function of the pump power. Insertion of (13.18) into (13.24) yields for the beam propagation factor:

$$M^2 = \frac{\pi b^2}{\lambda L^*} \sqrt{\frac{g_1^*(1-g_1^*g_2^*)}{g_2^*}} \left[ \left( 1 - \frac{d_1}{\rho_1} \right)^2 + \left( \frac{d_1}{L^*} \right)^2 \frac{g_1^*(1-g_1^*g_2^*)}{g_2^*} \right]^{-1} \quad (13.25)$$

This expression is only valid for  $M^2 > 1$  since lower beam quality factors make no physical sense. At the stability limits the beam quality factor approaches  $M^2=1$ . For rectangular active media, the radius  $b$  has to be replaced with half the side length. In general, the beam quality factors in the x- and the y-direction are different.

With the knowledge of the beam quality factor (13.25), the waist radii  $w_{mi}$  and the half angles of divergence  $\theta_{mi}$  can be calculated using (13.17) and (13.20):

$$w_{mi} = \sqrt{M^2} w_{0i}, \quad \theta_{mi} = \sqrt{M^2} \theta_{0i} \quad (13.26)$$

with the beam parameter product:

$$w\theta = w_{m1}\theta_{m1} = w_{m2}\theta_{m2} = M^2 \frac{\lambda}{\pi} \quad (13.27)$$

The locations of the waist radii are the same as for the Gaussian beam. It is interesting to note that the beam parameter product in multimode operation does not depend on the laser wavelength  $\lambda$ , since the beam quality factor scales with  $1/\lambda$ . We thus cannot improve the focusability by using a smaller wavelength. The beam parameter product of the Gaussian beam becomes lower with a smaller wavelength but the smaller Gaussian beam radius also

leads to the oscillation of a higher number of transverse modes. Therefore, the beam parameter product remains constant.

As previously discussed, the Gaussian beam radius in the medium exhibits a minimum near the center of a stable zone. Therefore, the multimode beam parameter product has a maximum at this point and decreases towards both stability limits. We can calculate the maximum beam parameter product by inserting (13.22) into (13.24):

$$(w\theta)_{\max} = k \frac{b^2 \Delta D}{4} \tag{13.28}$$

with:  $k = 1$  if the origin of the equivalent stability diagram is passed  
 $k = 2$  otherwise  
 $\Delta D$ : refractive power range within which the lens resonator is stable

Figure 13.7 presents the qualitative dependence of the beam parameter product on the refractive power for four different resonators with different refractive power ranges  $\Delta D$  and their different paths in the equivalent  $g$ -diagram. The beam parameter products in the unstable zones are not shown (it has not been determined how to calculate them at this time). This is not a disadvantage because the output power drops drastically as the resonators penetrate into unstable zones due to increasing diffraction losses at the active medium.

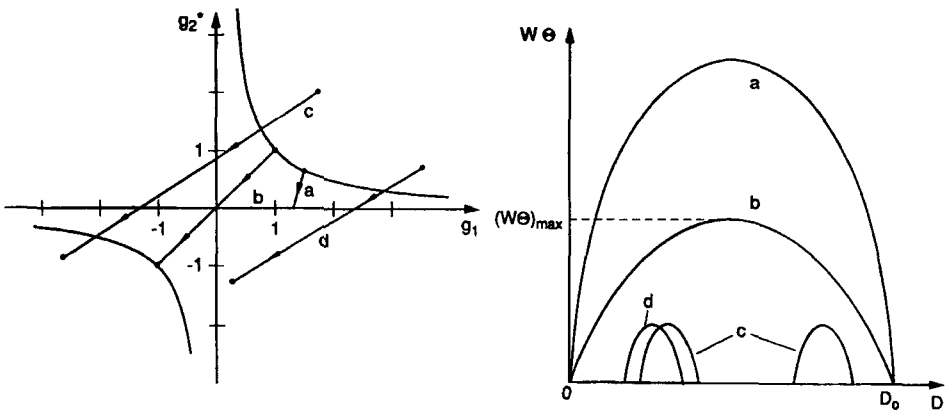


**Fig. 13.7** Qualitative dependence of the beam parameter product  $w\theta$  on the refractive power  $D$  for four resonators. In all resonators the thermal lens power is varied from  $\theta$  to  $D_0$ . Due to the different resonator geometries, the resonators pass through differently sized stable zones in the equivalent stability diagram.

In order to achieve a good beam quality, the resonator has to exhibit a small refractive range  $\Delta D$  within which it is stable. This is a problem in most cases since the refractive power of most solid state materials is relatively high, especially for those that provide high output power. In order to attain a certain beam quality it is therefore necessary to restrict the pump power range within which the laser is operated. A practical example may give a better understanding of this design problem.

**Example:**

A flashlamp-pumped Nd:YAG laser ( $\lambda=1.064\mu\text{m}$ ,  $n_0=1.82$ ) with a rod of length  $l=150\text{mm}$  and a radius of  $b=5\text{mm}$  is required to operate in a stable zone at 12kW of electrical pump power in order to obtain a high output power, but the beam parameter product should not exceed a value of 10 mm mrad at any pump power below 12kW. The refractive power of the rod was determined to be  $0.3\text{m}^{-1}$  per kW of pump power.

We choose a resonator that can pass through the origin of the stability diagram since then, according to (13.28), the largest stable zone for a given maximum beam parameter product is provided ( $k=1$ ). Equation (13.28) yields for the stable refractive power range  $\Delta D=1.6\text{m}^{-1}$ , a value that is much smaller than the total refractive power range of  $\Delta D_L=3.6\text{m}^{-1}$  of the laser rod. Since the lens resonator has to be stable at  $3.6\text{m}^{-1}$ , we chose a resonator which becomes stable at  $D_I=2.2\text{m}^{-1}$  and leaves the stable zone at  $D_{IV}=3.8\text{m}^{-1}$ . There is a whole variety of resonator set-ups that would fulfill this requirement; however, we use a symmetric resonator with two equal mirrors and the rod in the middle (Fig. 13.8). Equations (13.11) and (13.14) yield for the mirror curvatures  $\rho_1=\rho_2=-0.383\text{m}$  and for the distances  $d_1=d_2=0.526\text{m}$ . The geometrical length of the resonator is  $L_0=2d+(n_0-1)l/n_0=1.12\text{m}$ . Figure 13.8 presents the expected beam parameter products as a function of the refractive power. The laser can only be operated at pump powers between 7.35kW and 12.67kW.

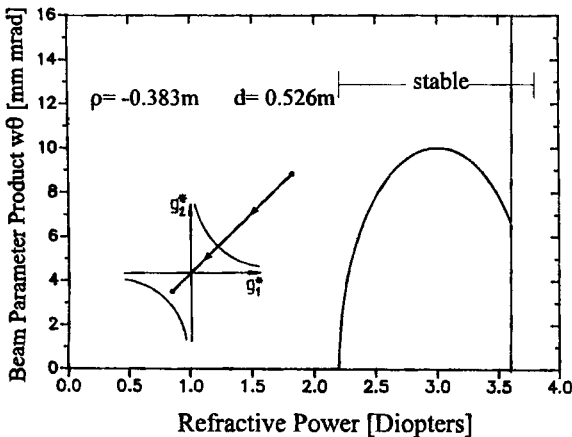


**Fig. 13.8** A symmetric resonator with mirror curvatures  $\rho_1=\rho_2=-0.383\text{m}$  and distances between the mirrors and the principal planes  $d_1=d_2=0.526\text{m}$  provides a maximum beam parameter product of 10 mm mrad for a Nd:YAG rod with a maximum refractive power of 3.6 Diopters.

As shown in the previous example, the laser resonator may not cover the whole stable refractive power range  $\Delta D$ , but only the portion  $\Delta D_A (=1.4m^{-1}$  in the example). How do we calculate the maximum beam parameter product in this case? Two cases have to be distinguished:

**a)  $\Delta D_A \geq \Delta D/2$**

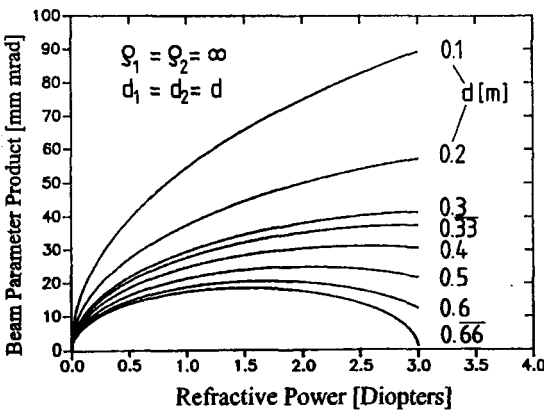
The maximum beam parameter product is given by (13.28)

**b)  $\Delta D_A < \Delta D/2$**

The maximum beam parameter product is lower than the one given by (13.28) since less than half the stable zone is covered by the lens resonator. To a good approximation the maximum beam parameter product can be calculated using:

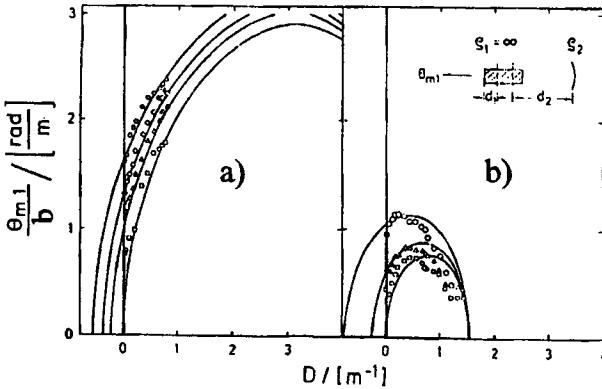
$$(w\theta)_{\max} = k \frac{b^2 \Delta D}{4} \left[ 1 - \left( 1 - \frac{2\Delta D_A}{\Delta D} \right)^2 \right] \tag{13.29}$$

Figure 13.9 presents a calculated example to clarify this statement. For a symmetric flat-flat resonator the beam parameter product is shown as a function of the refractive power. The curve parameter is the distance  $d$  from one mirror to the adjacent principal plane of the thermal lens. The operating range of the refractive power is  $\Delta D_A = 3m^{-1}$ . The refractive power range of the stable zone is given by  $\Delta D = 2/d$  and it decreases as the distance  $d$  is increased. For  $d < 1/3m$  the maximum beam parameter product given by (13.28) is reached, for larger distances the maximum beam parameter product is reached at the maximum refractive power, and it can be calculated with (13.29). This example also visualizes the typical dependence of the beam quality on the resonator length; low beam parameter products require long resonators.



**Fig. 13.9** Beam parameter product as a function of the refractive power for symmetric flat-flat resonators calculated with (13.25). The curve parameter is the distance  $d$  from one mirror to the adjacent principal plane of the laser rod (rod radius  $b=5mm$ ).

Figures 13.10 and 13.11 show measured beam divergences and beam parameter products for Nd:YAG rod lasers with different resonators in comparison with the theoretical curves given by (13.25) and (13.26). If the refractive power of the laser material is known, the theoretical values can be used to determine the beam quality with a good accuracy. On the other hand the measurement of the beam parameter product as a function of the pump power can be used to determine the refractive power (see also Chapter 23 for measurement techniques).



**Fig. 13.10** Measured half angles of divergence (normalized to the rod radius  $b$ ) of a Nd:YAG rod laser ( $b=3\text{mm}$ ,  $l=90\text{mm}$ ) with different plane-spherical resonators as a function of the refractive power of the rod. The curves were calculated using (13.25) and (13.26). a)  $d_2=0.165\text{m}$ , b)  $d_2=0.64\text{m}$ . The curve parameter is the radius of curvature  $\rho_2$  of the high reflecting mirror with:  $\square: \rho_2=\infty$ ,  $\Delta: \rho_2=5\text{m}$ ,  $\diamond: \rho_2=3\text{m}$ ,  $\circ: \rho_2=2\text{m}$ . The output coupling mirror is coated onto the left rod endface.

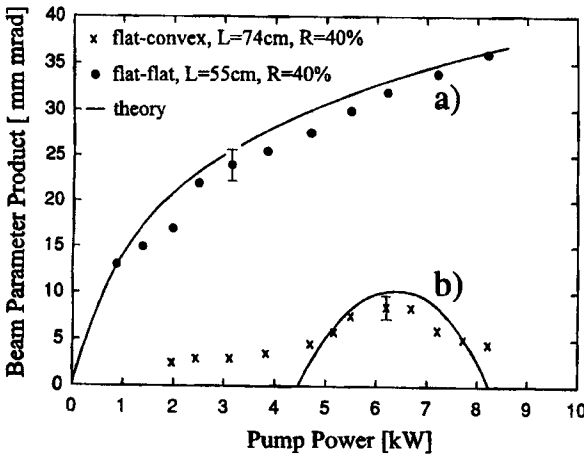


**Fig. 13.11** Measured and calculated beam parameter products of a Nd:YAG rod laser ( $b=10\text{mm}$ ,  $l=150\text{mm}$ ) for two resonators as a function of the pump power. a)  $d_1=d_2=0.24\text{m}$ ,  $\rho_1=\rho_2=\infty$  ; b)  $d_1=0.24\text{m}$ ,  $d_2=0.43\text{m}$ ,  $\rho_1=\infty$ ,  $\rho_2=-0.34\text{m}$ .

### 13.2.3 Beam Radii, Divergences, and Focusing

The thermal lens of the active medium has a considerable impact on the focusing properties of the laser beam. Since the beam waist, the angle of divergence and the position of the beam waist change with the refractive power, the size and the position of the focus spot vary as the pump power is increased (see Sec. 5.2.5). However, over large ranges of the refractive power either the waist radius or the angle of divergence stays fairly constant [4.91,4.93,4.99] (Fig. 13.12). If a flat output coupler is used, the position of the beam waist remains constant. Therefore, by using appropriate focusing optics in combination with a flat output coupler it is possible to maintain the position and the size of the focus over large ranges of the pump power.

If the waist radius is constant (first stable zone in Fig. 13.5), the beam can be focused to a spot of constant size by using a telescope as discussed in Sec.5.2.5. The telescope images the plane of the output coupling mirror to the plane of the focus spot; the focus is the image of the beam waist. The change in the divergence, therefore, will not affect the spot size. In areas of constant divergence, the preferred means of focusing is a focusing lens located at a distance of one focal length from the output coupling mirror. The spot size in the front focal plane only depends on the angle of divergence since the Fourier transform of the field at the output coupling mirror is generated.

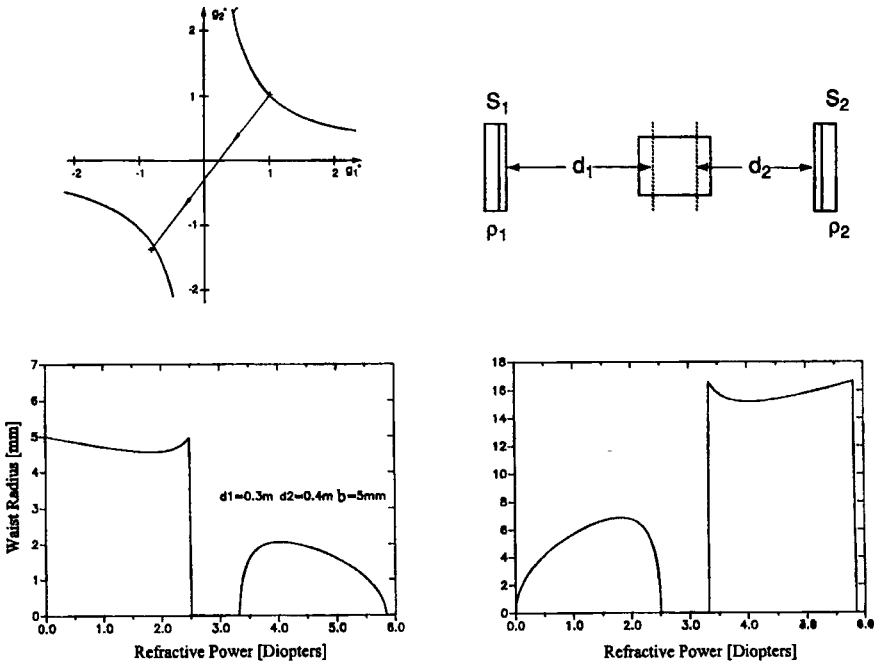
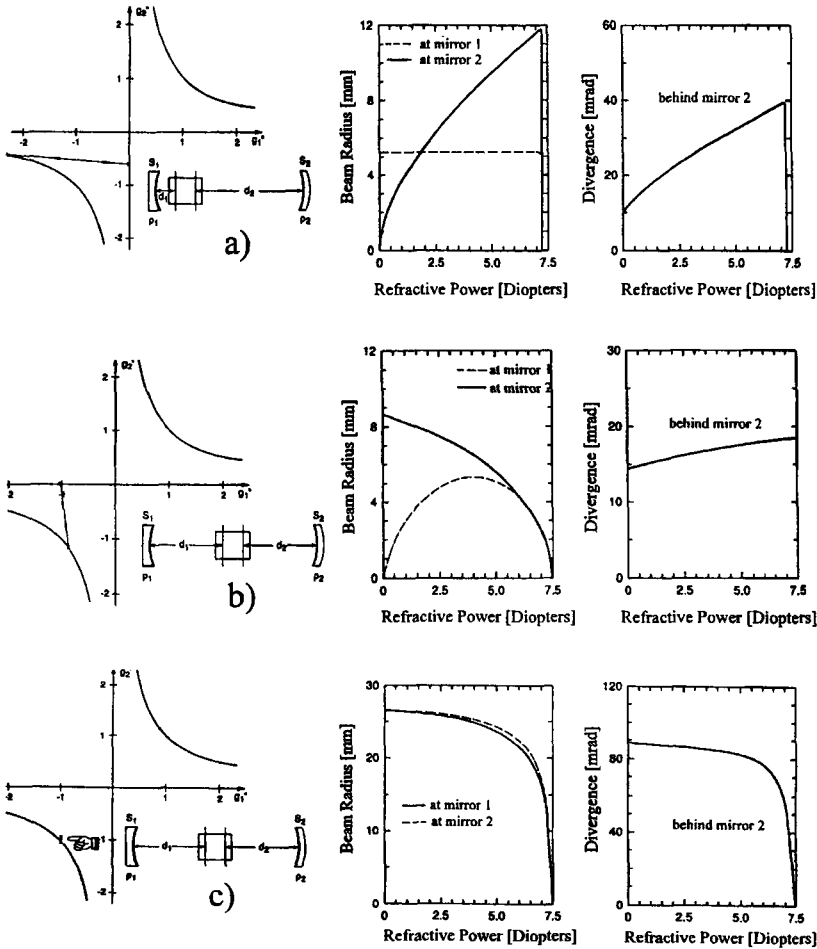


Fig. 13.12 Beam waist radius and half angle of divergence as a function of the refractive power for a flat-flat resonator. The output coupler is mirror 1 ( $b=5mm$ ,  $d_1=0.3m$ ,  $d_2=0.4m$ ,  $\lambda=1.064\mu m$ ).

Which of the two cases, constant waist radius or constant angle of divergence, is observed depends on the resonator set-up. If the output coupler is closer to the active medium than the high reflecting mirror, the waist radius stays constant in the first stable zone and the divergence in the second stable zone. This statement holds for all resonators with one flat mirror. If both mirrors are curved the waist position is a function of the pump power. However, we can still find regions of constant beam radius on one mirror or constant divergence (Fig. 13.13).



**Fig. 13.13** Calculated beam radii at the mirrors and angles of divergence behind mirror 2 as a function of the refractive power for three different resonators in the third quadrant of the stability diagram (rod radius  $b=5\text{mm}$ ,  $\lambda=1.064\mu\text{m}$ ). a)  $d_1=0.065\text{m}$ ,  $d_2=0.405\text{m}$ ,  $\rho_1=0.5\text{m}$ ,  $\rho_2=0.3\text{m}$ ; b)  $d_1=0.305\text{m}$ ,  $d_2=0.275\text{m}$ ,  $\rho_1=0.3\text{m}$ ,  $\rho_2=0.6\text{m}$ ; c)  $d_1=0.305\text{m}$ ,  $d_2=0.275\text{m}$ ,  $\rho_1=0.3\text{m}$ ,  $\rho_2=0.3\text{m}$ .

An interesting resonator is the one working close to the concentric point  $(-1,-1)$  in the equivalent  $g$ -diagram (Fig. 13.13c). Both the beam radius and the angle of divergence are relatively constant although refractive power is varied over a large range of 5 Diopters. This constancy is generated by the low sensitivity of the equivalent  $g$ -parameters to the refractive power; if we had a symmetric concentric resonator ( $d_1=d_2=\rho_1=\rho_2$ ) the equivalent  $g$ -parameters would not change at all. Unfortunately, the proportionality between the maximum beam parameter product and the stable refractive power range  $\Delta D$  also holds for this near concentric resonator. The price to pay for the beam radius and the divergence being constant simultaneously, therefore, is a high beam parameter product of 260 mm mrad.

### 12.2.4 Output Power and Beam Quality

Since the refractive power of a solid state laser is proportional to the pump power  $P_{pump}$ , we can find a relationship between the maximum beam parameter product and the pump power range  $\Delta P_{pump}$  within which the lens resonator is stable. Insertion of (13.5) into (13.28) yields [4.100]:

$$\frac{(w\theta)_{\max}}{\Delta P_{pump}} = k \frac{\alpha}{4\pi} \quad (13.30)$$

where  $\alpha$  is the thermal lensing coefficient,  $\Delta P_{pump}$  is the electrical pump power for flashlamp pumping and the absorbed optical pump power for diode pumping, and  $k=1$  if the confocal point is reached and  $k=2$  elsewhere. We thus need a small pump power range to realize good beam quality. Unfortunately, a small pump power range is related to a small output power range  $\Delta P_{out}$  since the resonator provides a useful output only inside the stable zones (Fig. 13.14):

$$\Delta P_{out} = \eta_{slope} \Delta P_{pump} \quad (13.31)$$

where  $\eta_{slope}$  is the slope efficiency (see Sec. 10.1.1). To obtain (13.31), we assumed that laser oscillation ceases once the stability limits are crossed. This assumption is not entirely correct as we shall see. Equation (13.30) can now be written as:

$$\frac{(w\theta)_{\max}}{\Delta P_{out}} = \frac{k}{4\pi} \frac{\alpha}{\eta_{slope}} \quad (13.32)$$

This expression reveals that a large range of the output power and a good beam quality cannot be achieved simultaneously. For a given excitation source (flashlamp or laser diode), the ratio of the thermal lensing coefficient to the slope efficiency can be considered a

characteristic for a solid state laser material (the maximum slope efficiency has to be used). This ratio can serve as a figure of merit for the high power performance of different solid state lasers. In order to combine a large output power range with a reasonable beam quality, materials with a low ratio are preferred. Tables 13.3 and 13.4 present values of  $\alpha/\eta_{slope}$  for common solid state materials.

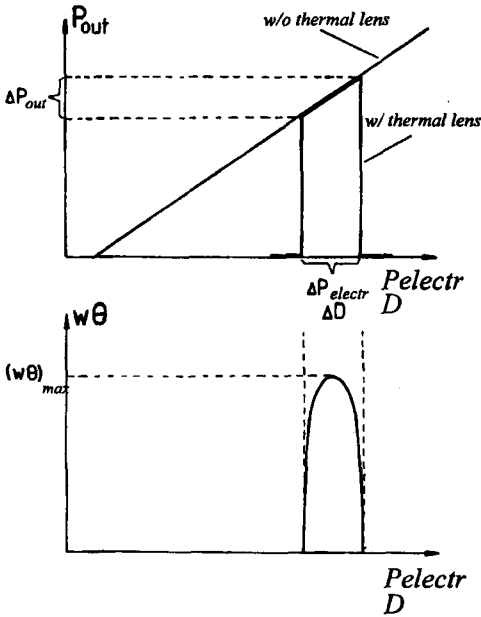


Fig. 13.14 With a thermal lens only the part of the output power curve can be used within which the resonator is stable. A small output power range is linked to a low maximum beam parameter product.

Table 13.3 Values of  $\alpha/\eta_{slope}$  in  $\mu\text{m}/\text{W}$  for flashlamp pumped solid state laser materials. Variations are due to differences in crystal quality, doping concentration, and slope efficiency.

Nd:YAG	Nd:glass	Nd:Cr:GSGG	Nd:Cr:GGG	Nd:YAP	Nd:YLF	Alexandrite
0.4-0.8	3.0-4.0	0.5-1.0	1.5-2.0	0.7-1.1	-(0.1-0.15)	0.2-0.3

Table 13.4 Values of  $\alpha/\eta_{slope}$  in  $\mu\text{m}/\text{W}$  for diode-pumped solid state laser materials. Variations are due to differences in doping concentration, absorption efficiency and pump geometry (see Table 13.2 for pump wavelengths).

Nd:YAG	Yb:YAG	Nd:YVO <sub>4</sub>	Nd:glass	Nd:YLF	Nd:YAP	Ti:sapphire
0.3-0.5	0.1-0.2	0.2-0.3	2.0-3.0	-0.05	0.5-0.75	0.25-0.35

Most commercially available solid state lasers are comprised of resonators that are either flat-flat or already stable at zero pump power. For these lasers the output power range is equivalent to the maximum output power. If we plotted the maximum beam parameter product of commercial Nd:YAG lasers as a function of the maximum output power we would thus expect a linear relationship. This is shown in Fig. 13.15 in comparison with the theoretical curve given by (13.32) with  $k=1$ . Beam quality and output power for diode-pumped single rod lasers are summarized in Fig. 13.16. Compared to flashlamp pumped systems, the beam parameter products are about 20% lower for the same output power, as expected from the values shown in Tables 13.2 and 13.3. The beam quality is generally worse than predicted by (13.32) due to two reasons. First, many commercial single rod systems do not use resonators that pass through the confocal point  $g_1^* = g_2^* = 0$ . The operation at this point is very sensitive to tolerances in the resonator design and small offsets of the mirror distances may result in a power dip.

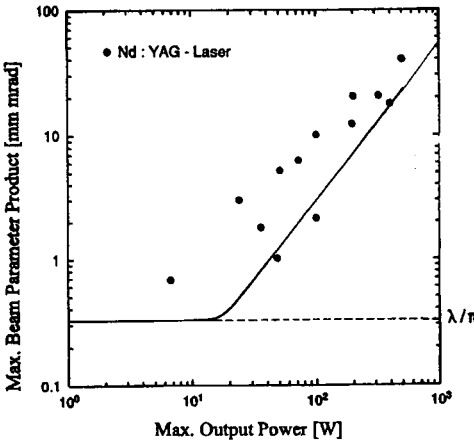


Fig. 13.15 Maximum beam parameter product as a function of the maximum average output power for commercially available flashlamp pumped single rod Nd:YAG lasers. The solid line represents (13.32) with  $k=1$ .

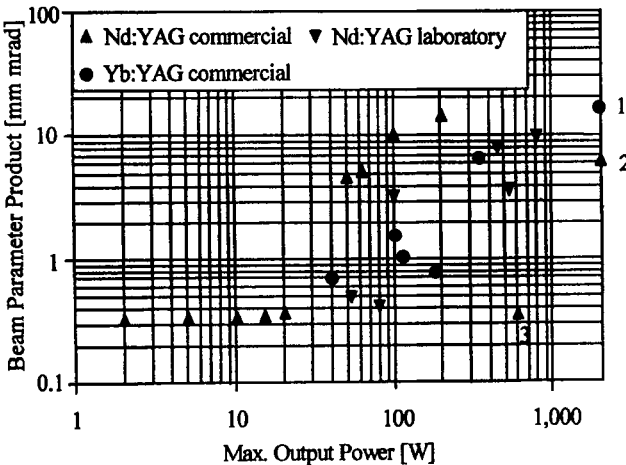
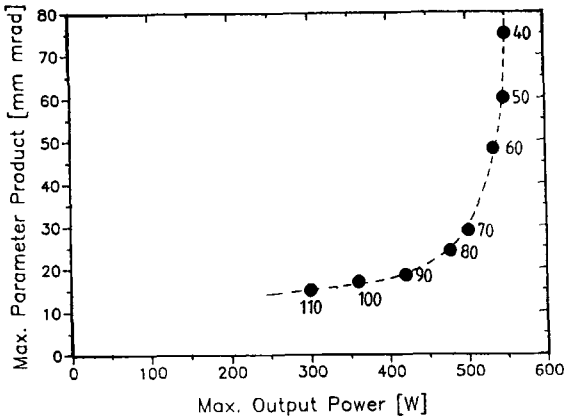


Fig. 13.16 Beam parameter products and output powers for diode-pumped solid state lasers using one Nd:YAG or Yb:YAG rod. For comparison: 1: fiber bundle laser, 2: disk laser with two disks, 3: single fiber laser



**Fig. 13.17** Measured maximum beam parameter products and maximum output powers for a pulsed flashlamp pumped Nd:YAG rod laser ( $b=5\text{mm}$ ,  $l=150\text{mm}$ ) with different symmetric flat-flat resonators. The number at each point is the geometrical resonator length in cm. The refractive power of the rod is  $0.38\text{m}^{-1}$  per kW of pump power and the pump power was varied between 0 and 12kW (pulse width: 2ms, pump energy: 240J, the repetition rate: 0-50Hz). The laser covers the whole stable zone ( $\Delta D=4.56\text{m}^{-1}$ ) for an effective resonator length of 93cm.

Secondly, commercial lasers generally do not cover the whole stable zone of the lens resonator. The reason for this is, besides space requirements, the decrease in laser efficiency when the lens resonator gets too close to a stability limit or the stable zone is chosen too small. As we shall see in the next section, this decrease is caused by spherical aberration of the thermal lens leading to a decrease of the fill factor. The modes basically "pull in their skirts" to avoid the strong aberration in the periphery of the medium. An experimental example is presented in Fig. 13.17 in which the maximum beam parameter product is plotted versus the maximum output power for a Nd:YAG laser with symmetric flat-flat resonators of different lengths. The maximum output power is decreased as the resonator length is increased. For a geometrical resonator length of 0.93m, the Nd:YAG laser would cover the whole stable zone with a maximum beam parameter product of 15mm mrad. Unfortunately, the output power is only 400W compared to 550W measured with a short resonator.

The beam quality of lens resonators can be improved by using a graded reflectivity mirror as an output coupler. The reflectivity profile acts as a mode-selecting aperture but in contrast to a conventional aperture, the power hitting the aperture is coupled out of the resonator. By using this technique it is possible to considerably enhance the beam quality of a lens resonator without decreasing the output power too much, as the experimental example in Fig. 13.18 indicates. This resonator scheme is, of course, also applicable to laser systems that do not exhibit thermal lensing.

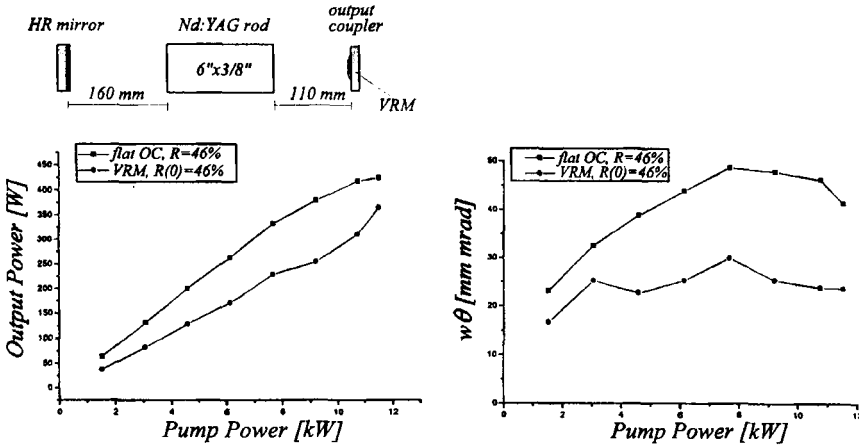


**Fig. 13.18** Measured output power (b) and measured beam parameter product (c) as a function of the electrical pump power for a pulsed, flashlamp pumped Nd:YAG rod laser utilizing the resonator set-up depicted in (a) ( $D=0.3$  diopters per kW of pump power). Measurements taken with a conventional flat output coupler ( $R=46\%$ ) and with a VRM with super-Gaussian index  $n=12$ , center reflectance  $R(0)=46\%$ , and a profile radius of  $w=2.5\text{mm}$  are compared. With the VRM, the beam parameter at the maximum output power is decreased by 45% whereas the output power drops only by 15% [S.12].

At the stability limits the lens resonator does not abruptly stop or start laser emission as was assumed in Fig. 13.14. If the resonator approaches a stable zone the output power begins to rise before the stability limit is crossed and a similar smoothing of the power curve is observed when the resonator goes unstable again. A typical example for this behavior is shown in Fig. 13.19 for a flashlamp pump Nd:YAG rod laser. The penetration of the power curve into the unstable zones is more pronounced the higher the small-signal gain of the laser. Since the diffraction losses are increased considerably as the resonator goes unstable, laser oscillation will stop as soon as the gain cannot compensate the losses anymore.

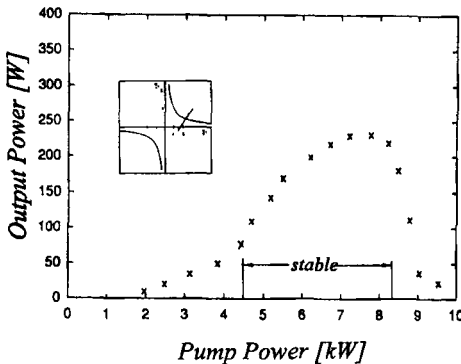


**Fig. 13.19** A lens resonator passes through a stable zone. The output power rises and falls outside the stability limits (pulsed Nd:YAG rod laser,  $b=5\text{mm}$ ,  $\ell=150\text{mm}$ , small-signal gain  $g_0\ell=4.1$ , mirror reflectance  $R=40\%$ ).

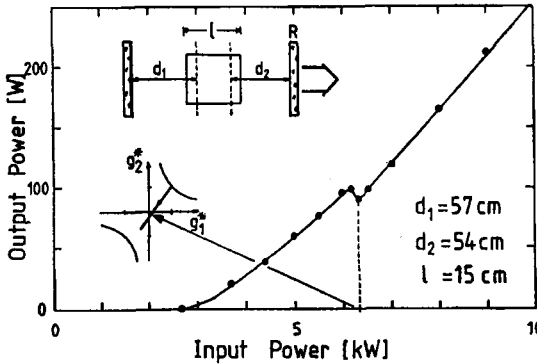


Fig. 13.20 Power dip generated by a small unstable zone. The lens resonator misses the confocal point due to the slight asymmetry of the resonator (pulsed Nd:YAG rod laser,  $b=5\text{mm}$ ,  $l=150\text{mm}$ , flat-flat resonator).

However, if the resonator only passes through a small unstable zone, as shown in Fig. 13.21, the output power may not go to zero at all. A dip in the output power is observed which can be used to determine the refractive power of the active medium. It should be added that the laser output in the unstable zones is not useful unless an output coupler with a confined high reflecting area (see Sec. 7.1) is used. We will discuss the operation in the unstable zones in Sec. 13.3.

In some cases, two power maxima are observed when the lens resonator penetrates into a wide enough unstable zone (Fig.13.21). The two maxima are generated if the laser material exhibits birefringence. For Nd:YAG the birefringence is caused by thermally induced stress; the refractive power for radially polarized light is about 15-20% higher compared to the refractive power for the azimuthal polarization. The radial polarization reaches the stability limit first and the output power drops as the refractive power is increased further. In the first power maximum the laser beam is radially polarized. Since resonator modes always try to decrease their losses, the polarization of the modes now becomes azimuthal. This polarization switching pushes the lens resonator back into the stable zone and, consequently, the output power rises again until the azimuthal polarization also goes unstable. Except for the operation at the limit of a stable zone, the laser beam is usually unpolarized, and the mean value of the two refractive powers can be used for the effective refractive power of the lens resonator.

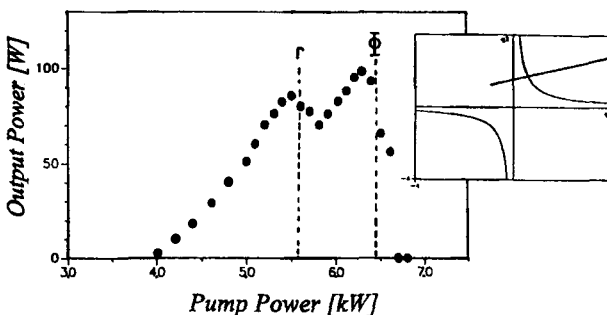


Fig. 13.21 Measured output power for a resonator with a small stability zone. The pump powers at which the second stability limit is reached are indicated for radial and azimuthal polarization (pulsed flashlamp pumped Nd:YAG rod laser,  $b=5\text{mm}$ ,  $l=150\text{mm}$ ,  $d_1=0.15\text{m}$ ,  $d_2=0.45\text{m}$ ,  $\rho_1=-0.3\text{m}$ ,  $\rho_2=-0.5\text{m}$ ).

### 13.2.5 Output Power in Fundamental Mode Operation

As discussed in Sec. 13.2.1, the Gaussian beam radius at the principal planes  $w_L$  exhibits a minimum  $w_{L,min}$  near the center of the stable refractive power range  $\Delta D$  with:

$$w_{L,min}^2 = \frac{4\lambda}{k \pi \Delta D} \tag{13.33}$$

with  $k=1$  if the confocal point  $g_1^* = g_2^* = 0$  is reached and  $k=2$  else. In order to attain fundamental mode operation an aperture with a radius  $a$  that is adapted to the Gaussian beam radius has to be placed in front of the medium:

$$a = x w_{L,min} , \quad x \in [1.3, \dots, 1.4] \tag{13.34}$$

Fundamental mode operation can be maintained over a refractive power range  $\Delta D_{00}$  which covers about 90% of the stable zone (Fig.13.22):

$$\Delta D_{00} = \frac{3.6 \lambda}{k \pi w_{L,min}^2} \tag{13.35}$$

Close to the stability limits the Gaussian beam radius  $w_L$  becomes much larger than the aperture radius and the resulting increase in the diffraction loss pushes the laser below threshold. In order to attain a high output power in fundamental mode operation, the Gaussian beam radius in the medium should be as large as possible. Unfortunately, (13.35) indicates that the refractive power range within which laser oscillation is achieved becomes smaller as the beam size is increased. For a typical Gaussian beam radius in a Nd:YAG laser rod of  $w_{L,min} = 1mm$ , (13.35) yields a refractive power range of 1.15 Diopters ( $k=1$ ).

We can rewrite (13.35) into a more convenient form by using the known expressions for the electrical pump power range and the output power range:

$$\Delta D_{00} = \frac{\alpha}{\pi b^2} \Delta P_{pump} \tag{13.36}$$

$$\Delta P_{out} = \frac{\alpha^2}{b^2} \eta_{slope} \Delta P_{pump} \tag{12.37}$$

- with
- $\alpha$  : thermal lensing coefficient (see Tables 13.1 and 13.2)
  - $b$  : rod radius
  - $\eta_{slope}$  : slope efficiency without aperture (multimode)

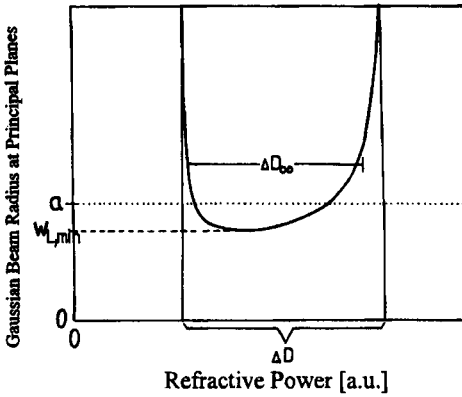


Fig. 13.22 Qualitative dependence of the Gaussian beam radius inside the medium on the refractive power. By limiting the medium with an aperture with radius  $a = 1.3w_{L,min}$ , fundamental mode operation is obtained within the range  $\Delta D_{00}$ .

Insertion of (13.34), (13.36), and (13.37) into (13.35) results in the following expression for the output power range (for  $a = 1.4 w_{L,min}$ ) [4.97]:

$$\Delta P_{out} = \frac{7.1 \lambda}{k} \frac{\eta_{slope}}{\alpha} \quad (13.38)$$

Again we find that the laser performance is determined by the ratio of the thermal lensing coefficient to the multimode slope efficiency.

Although the exact value of this ratio depends on the excitation source, the doping level, and the crystal quality, it can be considered a characteristic of a laser material. In order to attain a large power range in fundamental mode operation, this ratio has to be as small as possible. Tables 13.5 and 13.6 give an overview of the output power ranges in TEM<sub>00</sub> mode operation for different solid state materials for flashlamp pumping and diode pumping, respectively. Note that (13.38) represents the maximum output power if the resonator is already in a stable zone at zero pump power. Since most commercial fundamental mode lasers (mostly Nd:YAG lasers) are designed this way, the maximum fundamental mode power is on the order of 10-15W for flashlamp pumped systems [4.88,4.94,4.95,4.97] and about 20-25W for diode-pumped single rod lasers [4.115] (Fig.13.23). With the restriction that the resonator is stable at all pump powers, higher TEM<sub>00</sub> mode output power can only be realized if a laser material with better thermal properties, like Nd:YLF, is used. However, by limiting the stable zone of the resonator, it is possible to increase the output power in TEM<sub>00</sub> mode operation beyond the value given by (13.38). With diode-pumped single Nd:YAG rods, output powers of as high as 80W with  $M^2 < 1.2$  have been reported [4.112,4.113,4.117]. However, limitation of the stability zone does come at the cost of increased misalignment sensitivity and decreased overall efficiency. Figure 13.24 shows experimental results obtained with a side-pumped Nd:YAG using an intracavity 45° Faraday rotator for birefringence compensation [4.123]. The resonator is stable for pump powers between 660W and 725W, resulting in a TEM<sub>00</sub> mode beam diameter inside the rod of 1.7mm. At a pump power of 720W, the output power was 53W with an  $M^2$  of less than 1.5.

**Table 13.5** Output power range  $\Delta P_{out}$  in TEM<sub>00</sub> mode operation for different flashlamp pumped solid state laser materials ( $k=1$ ). The shown values correspond to the variations in  $\alpha/\eta_{slope}$ .

Material	wavelength $\lambda$ [ $\mu\text{m}$ ]	$\alpha/\eta_{slope}$ [mm/kW]	$\Delta P_{out}$ [W]
Nd:YAG	1.064	0.4 - 0.8	9.5 - 18.9
Nd:glass	1.054	3.0 - 4.0	1.9 - 3.5
Nd:Cr:GSGG	1.064	0.5 - 1.0	7.6 - 15.1
Nd:Cr:GGG	1.064	1.5 - 1.9	4.0 - 5.0
Nd:YAP	1.079	0.7 - 1.1	7.0 - 11.0
Nd:YLF	1.047	-(0.1 - 0.15)	50 - 75

**Table 13.6** Output power range in TEM<sub>00</sub> mode operation for different diode-pumped solid state laser materials ( $k=1$ ). The shown values correspond to the variations in  $\alpha/\eta_{slope}$ .

Material	wavelength $\lambda$ [ $\mu\text{m}$ ]	$\alpha/\eta_{slope}$ [ $\mu\text{m}/\text{W}$ ]	$\Delta P_{out}$ [W]
Nd:YAG	1.064	0.3 - 0.5	15.2 - 25.3
Yb:YAG	1.030	0.1 - 0.2	36.6 - 73.1
Nd:YVO <sub>4</sub>	1.064	0.2 - 0.3	22.8 - 28.4
Nd:glass	1.053	2.0 - 3.0	2.5 - 3.7
Nd:YAP	1.079	0.5 - 0.75	10.2 - 15.3
Nd:YLF	1.047	-(0.05 - 0.07)	103 - 148

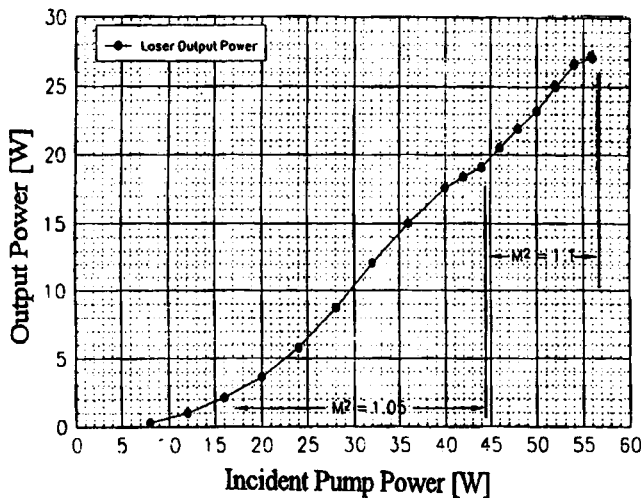


**Fig. 13.23** Measured output power in TEM<sub>00</sub> mode operation for a dual-diode-end-pumped Nd:YVO<sub>4</sub> laser with ~45cm long resonator as a function of the incident 808nm pump power. The laser emits a Gaussian mode over the entire output power range [4.115] (© SPIE 1998).

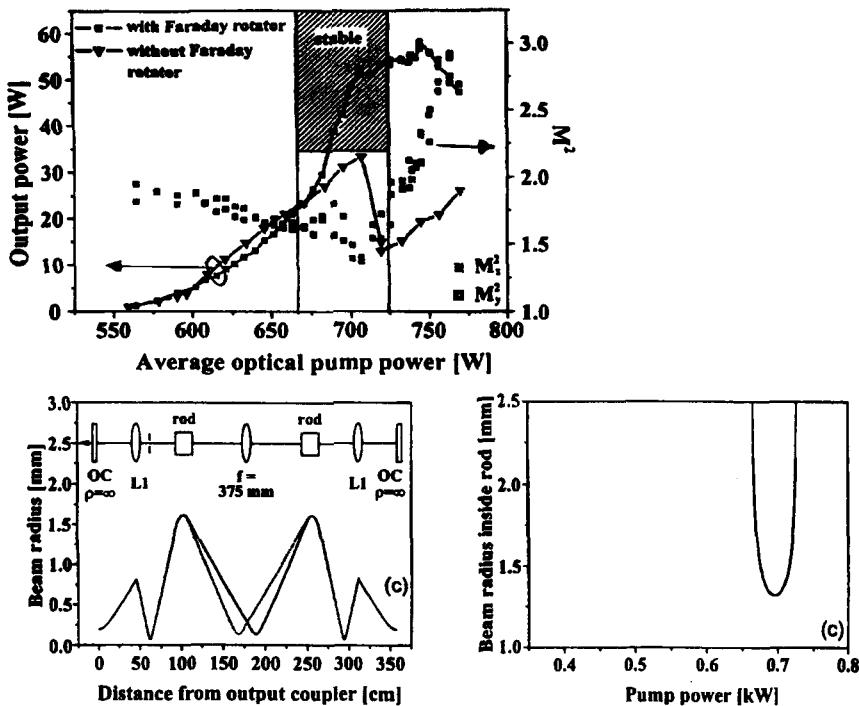


Fig. 13.24 Side-pumped Nd:YAG rod laser in  $TEM_{00}$  mode operation with restricted stable zone and birefringence compensation using a Faraday rotator. Measured output power and beam quality with and w/o the Faraday rotators are shown. The lower graphs depict the resonator set-up (presented for a round trip) and the calculated Gaussian beam diameter in the rod as a function of the pump power [4.117] (© OSA 2002).

### 13.2.6 Spherical Aberration

So far we only related the maximum beam parameter product to the output power range. This relationship does not inhibit the simultaneous realization of high output power and good beam quality as was shown in Fig. 13.24. Unfortunately, there is experimental evidence that the laser efficiency decreases considerably if the resonator operates close to a stability limit or if the stable zone is chosen small (Fig. 13.25). This decrease in efficiency is caused by the pump induced birefringence and by the spherical aberration of the thermal lens. Spherical aberration in solid state lasers is caused by inhomogeneous pump profiles and by the temperature dependence of both the thermal conductivity  $K$  and the thermo-optic constant  $dn/dT$ , resulting in a dependence of the refractive power on the radial coordinate. The refractive power in high power flashlamp or diode-side-pumped Nd:YAG lasers, for instance, typically is about 20-30% higher in the rod center. As a result, the diffraction

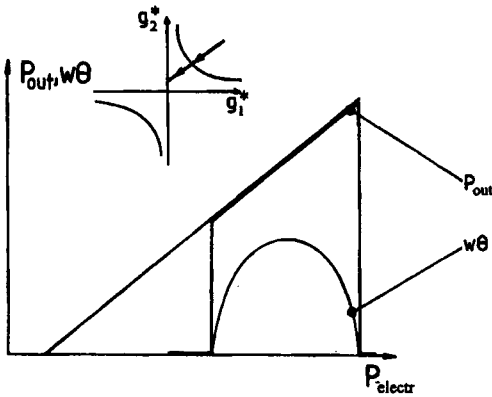


Fig. 13.25 High output power and a low beam parameter product should be attainable near a stability limit of the lens resonator.

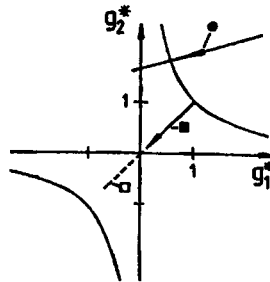
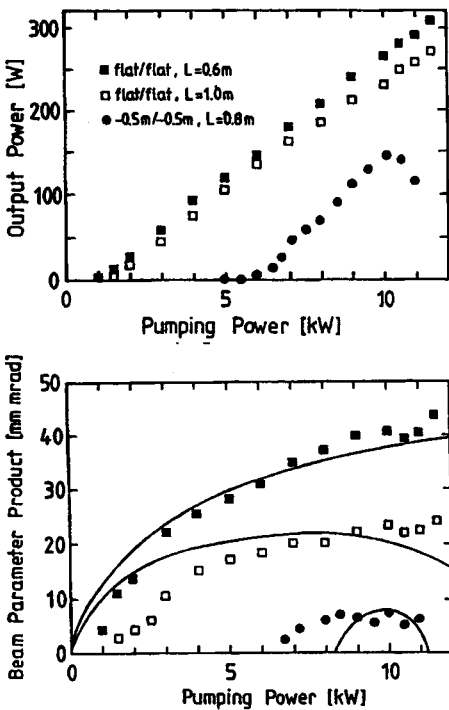


Fig. 13.26 Measured output power of a pulsed Nd:YAG rod laser ( $b=5\text{mm}$ ,  $l=150\text{mm}$ ,  $D=0.3\text{m}^{-1}$  per kW of pump power) as a function of the average pump power for three different resonators. A smaller stable zone results in a decrease of the output power. The beam parameter product  $w\theta$ , however, can still be calculated with Eq. (13.25) (solid lines in lower graph). The right graph shows the paths of the three resonators in the equivalent  $g$ -diagram [4.108] (© IEEE 1993).

losses become higher and the radius of the beam inside the medium decreases which means that the pump energy stored in the outer periphery of the rod is not being extracted anymore [4.109]. In the following we will derive an analytical expression for the spherically aberrated thermal lens as a function of the radial gain profile in the rod [4.82, 4.107]. Let us consider a rod with radius  $b$  and length  $\ell$  in which heat is generated at a rate  $Q$  per unit volume with a radial dependence given by (where the total heat is  $Q_0\pi b^2\ell$ ):

$$Q(r) = \frac{Q_0}{1 - \beta/2} \left( 1 - \frac{\beta}{b^2} r^2 \right) \tag{13.39}$$

This heat distribution is generated by a similar pump profile in the rod. For  $\beta=0$  the rod is pumped homogeneously, for  $\beta=0.5$  the gain at the center is twice as high as at the rod surface. The total heat  $P_H$  dissipated is independent of the shape parameter  $\beta$ :

$$P_H = \pi b^2 \ell Q_0 \tag{13.40}$$

The resulting temperature profile  $T(r)$  is a solution of the one-dimensional heat conduction equation which for a temperature dependent thermal conductivity  $K(T)$  reads:

$$\frac{1}{r} \frac{d}{dr} \left[ K(T) r \frac{dT}{dr} \right] = - Q(r) \tag{13.41}$$

For Nd:YAG, the thermal conductivity  $K(T)$  can be approximated by [4.108] (Fig.13.27):

$$K(T) = a/T, \quad \text{with } a = 36 \text{ W/cm} \tag{13.42}$$

Solving (13.41) for the radial temperature profile  $T(r)$  yields:

$$T(r) = - T_0 \exp \left[ \alpha \left[ 1 - \left( \frac{r}{b} \right)^2 - \frac{\beta}{4} \left[ 1 - \left( \frac{r}{b} \right)^4 \right] \right] \right] \tag{13.43}$$

with: 
$$\alpha = \frac{P_H}{4\pi a \ell (1 - \beta/2)} \tag{13.44}$$

$$T_0 = T_w + P_H / (2\pi b \ell h) \quad : \text{ surface temperature} \tag{13.45}$$

where  $T_w$  is the cooling water temperature and  $h$  is the heat transfer coefficient. The dissipated heat  $P_H$  is related to the electrical pump power  $P_{electr}$  (to the flashlamps or the diodes) via:

$$P_H = \chi \eta_{excit} P_{electr} \tag{13.46}$$

with  $\chi$ : thermal load parameter (=ratio of heat to power realized as inversion)  
 ~ 2.3-2.7 for pulsed flashlamp pumped Nd:YAG,  
 ~ 1.1-1.5 for cw flashlamp pumped Nd:YAG,  
 ~ 0.33 for diode-pumped Nd:YAG or Nd:YVO<sub>4</sub>)  
 $\eta_{excit}$ : excitation efficiency (see Sec. 9.3)  
 ~ 0.05-0.07 for flashlamp pumped Nd:YAG,  
 ~ 0.3 for end-pumped Nd:YAG or Nd:YVO<sub>4</sub>,  
 ~ 0.2 for side pumping

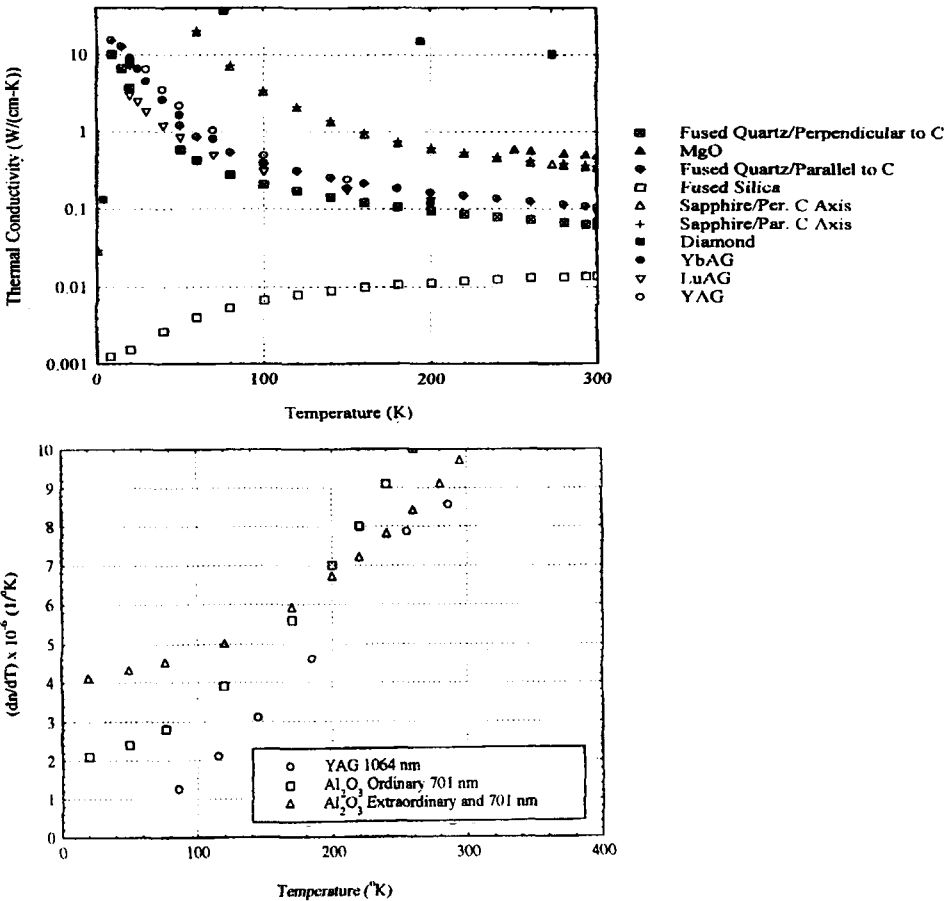


**Fig. 13.27** Measured temperature dependence of the thermal conductivity (top) and the thermo-optical constant  $dn/dT$  (bottom) for different dielectric materials and solid state laser hosts [S.34, S.35]. Courtesy of Dave Brown of Lynx Lasers, LLC.

Expansion of the exponential, neglecting terms with powers higher than 4, leads to:

$$T(r) = T_C \left[ 1 - \alpha \left[ \frac{r}{b} \right]^2 + \frac{\alpha^2}{2} \left[ 1 + \frac{\beta}{2\alpha} \right] \left[ \frac{r}{b} \right]^4 \right] \quad (13.47)$$

with: 
$$T_C = T_0 \exp \left[ \alpha \left( 1 - \frac{\beta}{4} \right) \right]$$

The refractive power of the thermal lens is given by:

$$D(r) = - \ell \frac{dn}{dT} \frac{d^2 T(r)}{dr^2} \quad (13.48)$$

where  $dn/dT$  is the thermo-optical constant (temperature derivative of the index of refraction), which is also a function of the temperature (Fig.13.27):

$$\frac{dn}{dT} = \epsilon + \delta (T(r) - T_w) \quad (13.49)$$

where  $\epsilon$  is  $dn/dT$  at the water temperature  $T_w$  and  $\delta$  is the slope of the curve in Fig.13.27 ( $=d^2n/dT^2$ ). Due to the non-parabolic temperature profile and the temperature dependence of  $dn/dT$ , the refractive power is a function of the radius. This means that an incident ray parallel to the optical axis at a distance  $r$  will intersect the optical axis at a distance  $1/D(r)$  from the principal plane of the thermal lens. Inserting (13.49) and (13.47) into (13.48) and neglecting terms depending on a power of the radius higher than 4, the final result for the refractive power reads:

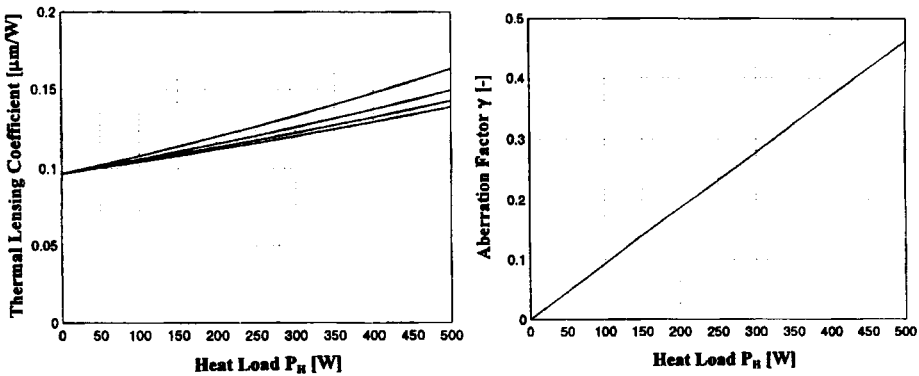
$$D(r) = D_0 \left[ 1 - \gamma \left( \frac{r}{b} \right)^2 \right] \quad (13.50)$$

with: 
$$D_0 = \frac{2\ell\alpha T_C}{b^2} [\epsilon + \delta(T_C - T_w)] \quad : \text{center refractive power} \quad (13.51)$$

$$\gamma = \frac{3}{2}\beta + \alpha \left( 3 + \frac{\delta T_C}{\epsilon + \delta(T_C - T_w)} \right) \quad : \text{aberration factor} \quad (13.52)$$

The refractive power decreases parabolically with the radius and since both  $\alpha$  and  $T_C$  are a non-linear function of the heat load  $P_H$ , both the center refractive power  $D_0$  and the aberration factor  $\gamma$  show a non-linear increase with pump power. Figure 13.28 shows calculated center refractive powers and aberration factors for a diode side-pumped Nd:YAG

laser rod as a function of the heat load for different rod diameters, assuming a homogeneous heat distribution in the rod ( $\beta=0$ ). Measured radial dependence of the refractive power of a flashlamp pumped Nd:YAG laser are depicted in Fig. 13.29. The nonlinear increase of the refractive power with the pump power can be easily observed in diode end-pumped TEM<sub>00</sub> mode solid state lasers because high pump power of tens of Watts is deposited in small pump spot diameters of typically less than 1 mm (Fig. 13.30). The nonlinear increase of the refractive power in combination with the strong aberration of the thermal lens severely limits the power scalability of these systems. Power scaling therefore requires optimization of the pump geometry by reducing the heat load (e.g. 880nm instead of 808nm pumping for Nd:YVO<sub>4</sub>) and reducing the doping concentration while keeping the overall pump light absorption high.



13.28 Calculated thermal lensing coefficient  $D_0\pi b^2/P_{\text{abs}}$  and aberration factor  $\gamma$  for homogeneously diode-pumped Nd:YAG rods of 10 cm length as a function of the heat load  $P_H$  and different rod diameters (using (13.51) and (13.52)). Rod diameters  $2b$  are 4, 6, 8, and 10 mm from bottom to top. ( $\beta=0$ ,  $\epsilon=9.5 \cdot 10^{-6} \text{ 1/K}$ ,  $\delta=0.04 \cdot 10^{-6} \text{ 1/K}^2$ ,  $T_w=293\text{K}$ ,  $h=1.0 \text{ W}/(\text{cm}^2 \text{ K})$ ,  $P_H=0.25 \cdot P_{\text{abs}}$ ,  $P_{\text{abs}}$ : absorbed pump power at 808nm).

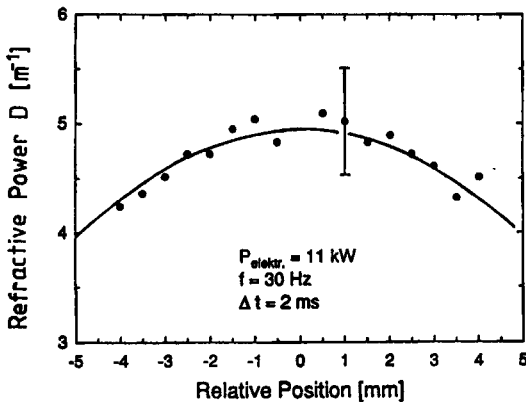
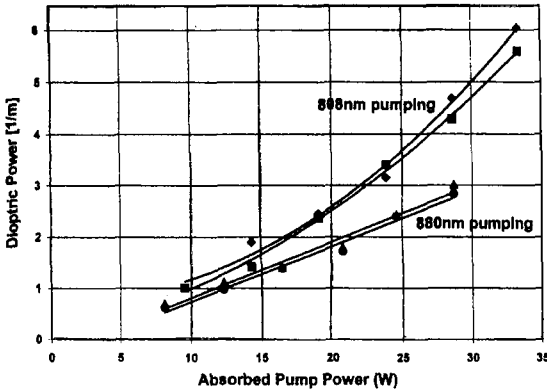


Fig. 13.29 Measured radial profile of the refractive power for a dual flashlamp pumped pulsed Nd:YAG laser rod (10mm diameter) in a ceramic pump cavity for 11kW average electrical pump power. The specular reflection of ceramic generates a nearly homogeneous pump profile in the rod. The solid line represents (13.50) with  $\gamma=0.2$  [4.108] (© IEEE 1993).



**Fig. 13.30** Measured dioptric power at 1064nm of a 15mm long end-pumped Nd:YVO<sub>4</sub> crystal with 0.4at% doping as a function of the absorbed pump power for different diode pump wavelengths. The pump spot diameter is 1.1mm. The 40% higher heat load for 808nm pumping and the shorter absorption lengths leads to a nonlinear increase of the thermal lensing due to the increased temperature [S.32]. For each pump wavelength, the two curves represent measurements in x- and y-direction, respectively.

Equations (13.50-13.52) reveal important properties of spherical aberration in pumped rods:

- the refractive power decreases parabolically with the radius. A constant refractive power can only be achieved if the pump profile exhibits a minimum at the center; for flashlamp pumped systems this is very difficult if not impossible to realize.
- the spherical aberration is also present for homogeneous pumping. For a homogeneously pumped, 150 mm long, Nd:YAG rod, the aberration factor  $\gamma$  is about 0.4 per kW of dissipated heat.
- the aberration factor  $\gamma$  is proportional to the dissipated heat, which means aberration becomes stronger as the pump power is increased.
- the aberration factor  $\gamma$  is inversely proportional to the rod length. Therefore, it is advantageous to use longer rods, which for end-pumped systems means that the doping concentration has to be decreased proportionally.
- the aberration factor  $\gamma$  does not depend on the rod radius ! Although a bigger rod will exhibit a lower center temperature, the relative radial decrease of the refractive power is the same.

In other words, spherical aberration of the thermal lens basically is always noticeable in medium to high power solid state lasers. In multimode lasers, however, this causes problems only near the unstable zones. The typical influence of the spherically aberrated lens on the resonator performance is shown in Fig. 13.31. The calculated output power and beam quality factor of three resonators all having flat rear mirrors but different lengths and output coupler curvatures are compared. The small-signal gain was kept constant and the refractive power was increased up to 2 Diopters. Without aberration ( $\gamma=0$ ), the output power remains constant if the stable range  $\Delta D$  is decreased and the beam quality factor shows the expected parabolic dependence on the refractive power. With aberration ( $\gamma=0.45$ ), the output power is reduced significantly for the resonators with smaller stable zones. The effect on the beam quality is less dramatic, but note that the beam quality is improved by aberration due to a lower fill factor [4.110,4.124]. These theoretical results seem to be in good agreement with the experimental results presented in Figs.13.32 and 13.33.

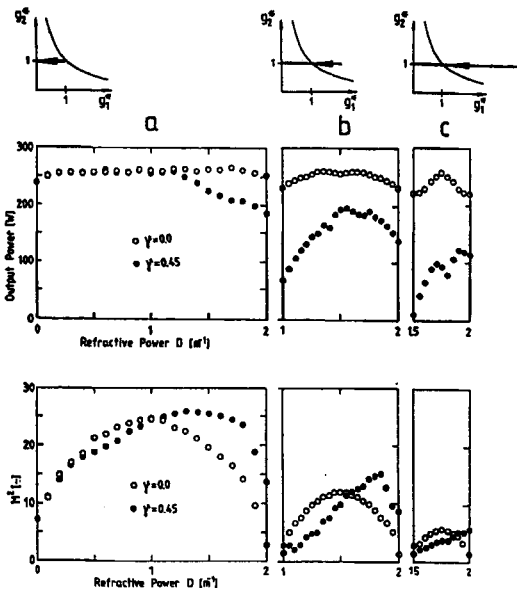


**Fig. 13.31** Calculated output power and beam quality factor with ( $\gamma=0.45$ ) and without aberration ( $\gamma=0.0$ ) for resonators covering different large stable zones in the stability diagram. The gain medium with radius  $b=3\text{mm}$ , wavelength  $\lambda=1.064\mu\text{m}$ , and loss factor per transit  $V_S=0.95$  is located at the output coupling mirror 1 ( $R=80\%$ ) and exhibits a small-signal gain of  $g_0\ell=1.0$  ( $I_S=2\text{kW/cm}^2$ ). a)  $\rho_1=\rho_2=\infty, d_1=0\text{m}, d_2=0.5\text{m}$ , a)  $\rho_1=-0.5\text{m}, \rho_2=\infty, d_1=0\text{m}, d_2=1.0\text{m}$ , a)  $\rho_1=-0.66\text{m}, \rho_2=\infty, d_1=0\text{m}, d_2=2.0\text{m}$  [4.108] (© IEEE 1993).

A drastic experimental example of how the output power drops off if the stable refractive power range  $\Delta D$  is chosen small is presented in Fig. 13.32. This resonator exhibits two stable zones of less than 0.3 Diopters, located at high input power. Compared to a short flat-flat resonator, the output power is decreased by one order of magnitude. The different power maxima correspond to different polarizations of the radiation. The resonator reaches the first stable zone with a mode structure mainly radially polarized. Before the resonator goes unstable, the polarization is changed to azimuthal orientation and a second power peak is observed. In the second stable zone, the stable refractive power range  $\Delta D$  is larger than the difference of refractive powers of the two polarizations. As a consequence, the two power maxima are not separated anymore (third peak).

Due to spherical aberration and birefringence, high output power is always linked to a deterioration of the beam quality, if common dual-mirror resonators without internal lenses are used. For each output power a lower bound for the beam parameter product exists. This is shown in Fig. 13.33 for a Nd:YAG laser capable of a maximum average output power of 320W. The beam parameter products for a variety of resonators are plotted versus the output power. The minimum beam parameter product observed increases considerably if the maximum output power is approached. Even for low output powers between 50 and 100W it is not possible with this laser to get a beam quality better than 13 times diffraction limited.

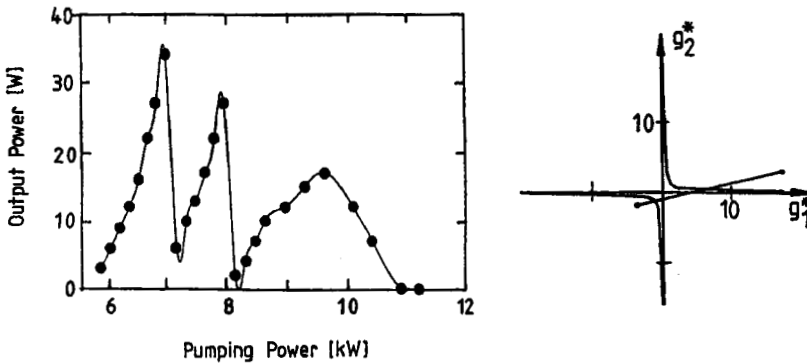


**Fig. 13.32** Measured output power of a pulsed Nd:YAG rod laser ( $b=5\text{mm}$ ,  $\ell=150\text{mm}$ ) utilizing a resonator with two extremely small stable zones as a function of the electrical pump power. The right graph shows the stability diagram for a pump power range of 12kW. The power maxima are related to different polarizations. Resonator data:  $\rho_1=-0.09\text{m}$ ,  $\rho_2=-0.65\text{m}$ ,  $d_1=76\text{cm}$ ,  $d_2=79\text{cm}$ ,  $R=80\%$ , input energy: 80J, pulse duration: 2ms, repetition rate is varied from 0 to 150 Hz, refractive power: 0.3 Diopters per kW of pump power [4.108] (© IEEE 1993).

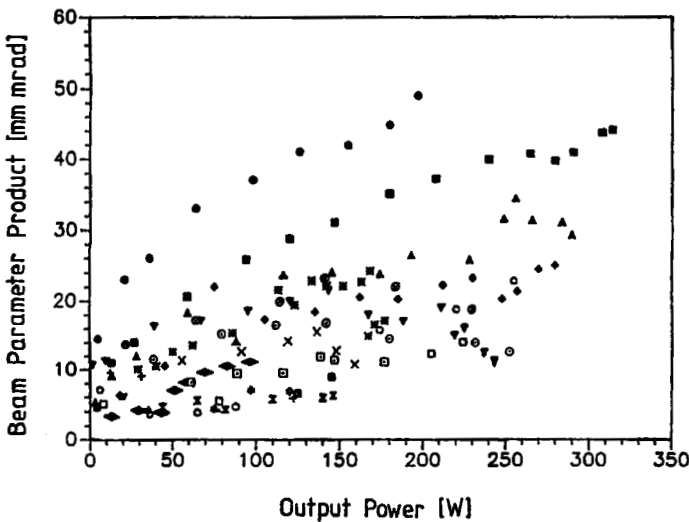


**Fig. 13.33** Measured beam parameter product  $w\theta$  versus measured output power for a Nd:YAG rod laser ( $b=5\text{mm}$ ,  $\ell=150\text{mm}$ ,  $D=0.3\text{m}^{-1}$  per kW of pump power), using 15 resonators with differently large stable zones in the stability diagram. (repetition rate: 30Hz, pulse width: 2ms, input energy was varied from 0 to 400J). The following resonator data  $\rho_1/\rho_2/d_1/d_2$  were used: ●:  $\infty/\infty/13\text{cm}/13\text{cm}$ ; ■:  $\infty/\infty/23\text{cm}/23\text{cm}$ ; ▲:  $\infty/\infty/33\text{cm}/33\text{cm}$ ; ◆:  $\infty/\infty/43\text{cm}/43\text{cm}$ ; ▼:  $\infty/\infty/54\text{cm}/54\text{cm}$ ; ○:  $\infty/\infty/59\text{cm}/59\text{cm}$ ; ○:  $\infty/\infty/63\text{cm}/63\text{cm}$ ; □:  $\infty/\infty/66\text{cm}/66\text{cm}$ ; \*:-0.5m/ $\infty/20\text{cm}/45\text{cm}$ ; ○:-0.3m/ $\infty/13\text{cm}/33\text{cm}$ ; □:-0.3m/ $\infty/43\text{cm}/43\text{cm}$ ; X: -0.5m/-0.5m/21cm/21cm; ☆:-0.3m/-0.5m/10cm/40cm; X: -0.3m/ $\infty/10\text{cm}/83\text{cm}$ ; ◆:-1m/ $\infty/90\text{cm}/53\text{cm}$  [4.108] (© IEEE 1993).

The temperature induced part of spherical aberration in laser rods is, according to (13.51/13.52), inversely proportional to the rod length  $l$ . Therefore, it is possible to attain a higher output power at the same beam quality by distributing the pump power over a longer active medium. Since the available crystal lengths are limited to 200mm, the preferred arrangement is a dual rod resonator that exhibits small refractive power ranges within which the resonator is stable. A quartz rotator (QR) between the rods is used for birefringence compensation so that the resonator stability does not depend on the polarization of the resonator modes. The Nd:YAG laser resonator depicted in Fig. 13.33 utilizes two 150mm long flashlamp pumped Nd:YAG rods to provide a maximum output power of 290W and a beam parameter product of 1.25 mm mrad ( $M^2=3.75$ ) at a total electrical pump power 14.3kW. Although the output power is less than half the maximally possible (a short flat-flat resonator provides 650W at the same pump power), the beam parameter product at this output power could be decreased several times, compared to a single rod resonator providing the same output power. In recent years, similar set-ups have been used to improve the brightness of diode-pumped Nd:YAG lasers:  $M^2=4, P=500W$  [4.121],  $M^2<1.1, P=208W$  [4.116],  $M^2=1.2, P=183W$  [4.123],  $M^2<1.2, P=153W$  [4.120]. With an Yb:YAG dual rod system,  $M^2$  of 2.2 at an output power of 530W was measured [4.118,4.119].

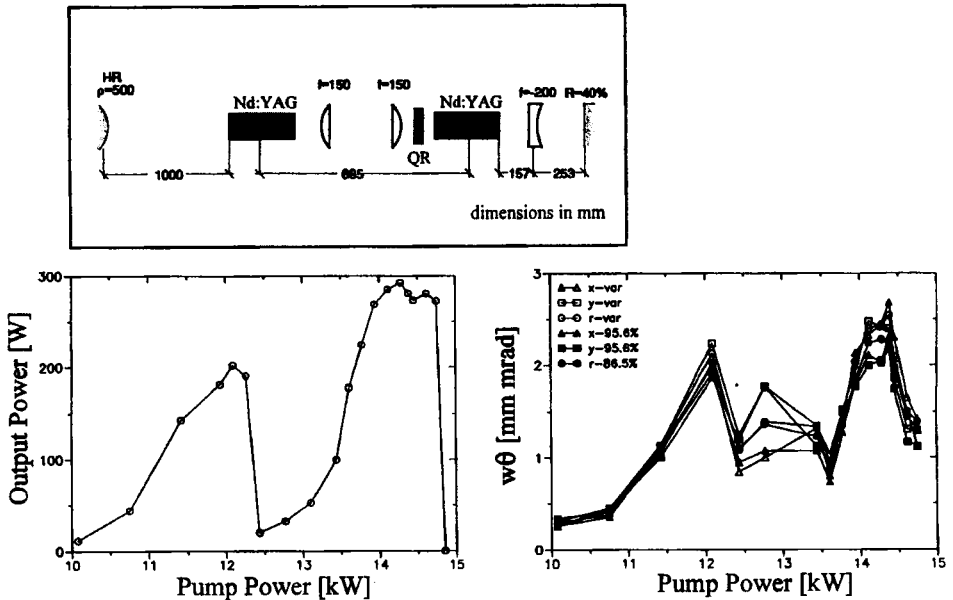
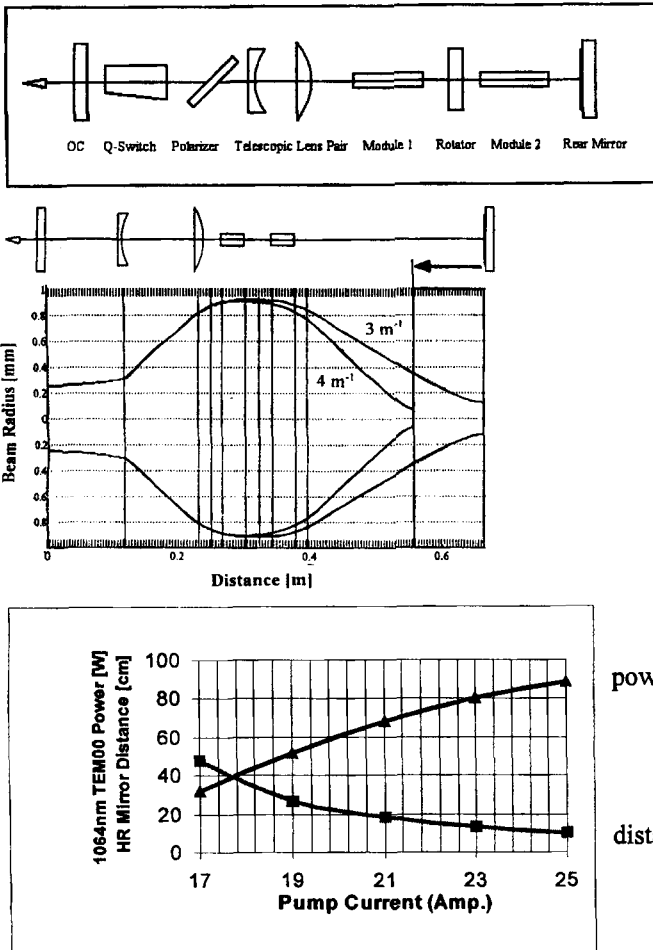


Fig. 13.33 Resonator set-up, measured output power and measured beam parameter product as a function of the total electrical pump power for a pulsed, dual rod Nd:YAG laser ( $b=4.75mm$ ,  $l=150mm$ , refractive power per rod:  $0.28m^{-1}$  per kW of pump power). Pump energy per rod : 168J, pump pulse duration: 4ms, maximum repetition rate: 44 Hz. The beam parameter products (waist radius  $w$  times half angle of divergence  $\theta$ ) defined via the power content (full points) and via the second intensity moment (open points) are shown [S.13].

In all of these demonstrations of high power TEM<sub>00</sub> mode operation, resonators were used that operated only within a limited pump power range. This restriction can be overcome by moving one of the resonator mirrors inwards as the pump power is increased. This way TEM<sub>00</sub> mode operation can be attained at all pump power levels, and the beam diameter in the active media and on one of the resonator mirrors can be kept constant. An experimental realization of this technique in an industrial diode-pumped Nd:YAG laser is shown in Fig. 13.34.



**Fig. 13.34** Side-pumped dual rod Nd:YAG laser with moving HR mirror to compensate for a varying refractive power per rod. The middle graph shows the calculated TEM<sub>00</sub> mode beam diameter for 3 and 4 Diopters of refractive power per rod. The lower graph depicts measured TEM<sub>00</sub> mode power (upper curve) and the distance of the HR mirror from the adjacent rod end face as a function of the diode current. A current of 25A is equivalent to an optical pump power of 300W per rod. By moving the HR mirror, the TEM<sub>00</sub> mode diameters at the output coupler and inside the rods remain constant with varying pump power [4.125,S.33].

The aberration of the thermal lens can lead to a significant decrease of the beam quality when near diffraction limited beams are amplified. For a transit in the amplifier, the phase shift generated by the thermal lens is given by:

$$\Delta\Phi(r) = \frac{2\pi}{\lambda} \left[ \frac{D(r) r^2}{2} \right] = \frac{2\pi}{\lambda} \left[ \frac{D_0 r^2}{2} - \frac{D_0 \gamma r^4}{2b^2} \right] \tag{13.53}$$

Neglecting gain saturation effects, the beam propagation factor  $M^2$  of the amplified beam can be calculated by using the second intensity moments (see Sec. 2.6.2):

$$M^2 = \frac{\pi}{\lambda} \sqrt{\langle w^2 \rangle \langle \theta^2 \rangle - \langle w\theta \rangle^2} \tag{13.54}$$

For radially symmetric beam with Gaussian intensity profile and initial beam propagation factor  $M_i^2$ , the beam propagation factor  $M_f^2$  after amplification reads [4.115,4.126]:

$$M_f^2 = \sqrt{\left[ M_i^2 \right]^2 + \left[ \frac{\sqrt{8} \alpha_T P_{abs} \gamma}{\lambda} \left( \frac{w}{b} \right)^4 \right]^2} \tag{13.55}$$

where  $\alpha_T$  is the thermal lensing coefficient ( $=D_0 \pi b^2 / P_{abs}$ ) and  $P_{abs}$  is the absorbed pump power. Figure 13.35 shows a calculated example for a diode-pumped Nd:YAG rod.

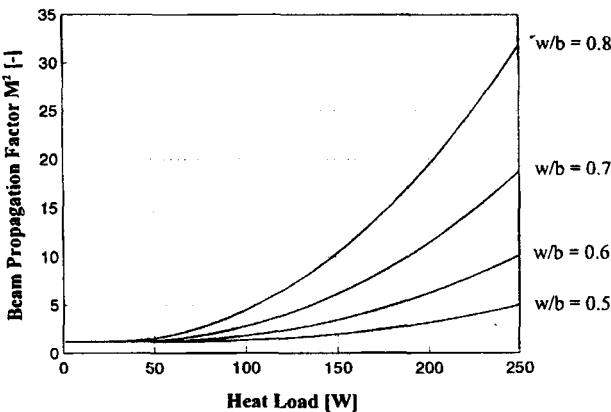


**Fig. 13.35** Calculated beam propagation factor  $M_f^2$  of an incident  $TEM_{00}$  mode beam ( $M_i^2=1.2$ ) after propagation through a homogeneously diode-pumped Nd:YAG rod amplifier with 4mm diameter and 10 cm length as a function of the heat load  $P_H$ , using (13.51,13.52 and 13.55). Curve parameter is the ratio of beam radius  $w$  to rod radius  $b$ . ( $\beta=0$ ,  $\epsilon=9.5 \cdot 10^{-6}$  1/K,  $\delta=0.04 \cdot 10^{-6}$  1/K<sup>2</sup>,  $T_w=293$ K,  $h=1.0$  W/(cm<sup>2</sup> K)  $P_H=0.25 \cdot P_{abs}$ ,  $P_{abs}$ : absorbed pump power at 808nm).

### 13.3 Unstable Resonators

#### 13.3.1 Beam Propagation

In unstable resonators the refractive power of the thermal lens leads to a decrease of the magnification  $M$  and of the equivalent Fresnel number  $N_{eq}$ . Furthermore, the radius of curvature of the outcoupled wavefront is a function of the refractive power, which means that the location of the focus spot changes as the pump power is increased [4.39,4.104,4.130]. The concept of the equivalent resonator discussed in the preceding section is also applicable to unstable resonators. The unstable lens resonator with  $g$ -parameters  $g_1, g_2$  and distances  $d_1, d_2$  from the mirrors to the principal planes of the lens exhibits the same field distributions at the resonator mirrors and the same output coupling loss as the equivalent, empty resonator with  $g$ -parameters  $g_1^*, g_2^*$  and the geometrical length  $L^*$  (see Eqs. (13.8)-(13.10)).

Figure 13.36 presents the typical behavior of an unstable lens resonator. In this example the thermal lens with a refractive power between 0 and 3.1 Diopters is located at the high reflecting mirror 2. Therefore, the  $g$ -parameter of the output coupling mirror stays constant. In order to stay in the unstable zone over the whole refractive power range, the resonator has to start at a high magnification of  $M=24.2$ . The magnification is decreased down to  $M=1.0$  as the resonator travels towards the stability limit with increasing refractive power. The beam propagation shown for three refractive powers demonstrates the sensitivity of the magnification and of the position of the focus spot to the refractive power. It is evident that this resonator can only be operated efficiently over a small refractive power range around the confocal point at  $D=3m^{-1}$  at which a magnification of  $M=2$  is attained. Fortunately, the sensitivity can be decreased considerably by choosing a proper resonator design.

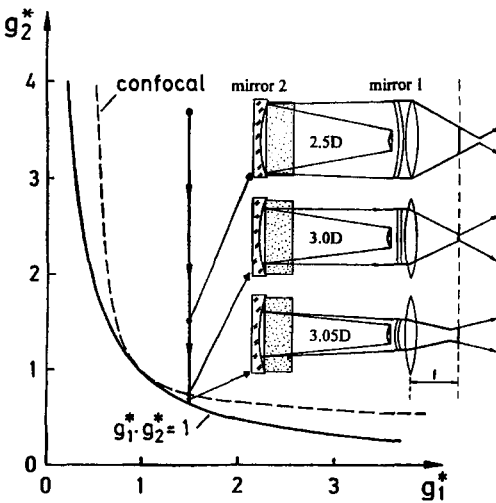


**Fig. 13.36** The equivalent  $g$ -diagram for a positive branch unstable resonator ( $\rho_1 = -2m$ ,  $\rho_2 = -0.364m$ ,  $d_1 = 1.0m$ ,  $d_2 = 0$ ). The refractive power is varied between 0 and  $3.1m^{-1}$ . The beam propagation including focusing is shown for three refractive powers. The resonator is confocal at  $3.0m^{-1}$  with a magnification of  $M=2$ .

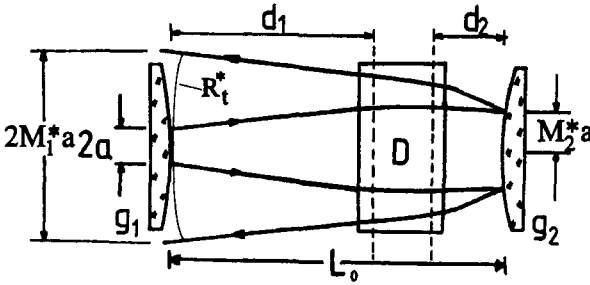


Fig. 13.37 Beam propagation in an unstable resonator with a variable lens.

All relations derived in Sec.7, except for the wavefront curvatures, are still valid for the unstable lens resonators if the equivalent resonator parameters  $g_1^*, g_2^*, L^*$  are inserted (Fig.13.37):

$$\text{Equivalent } g\text{-parameters} \quad : \quad g_i^* = g_i - Dd_j \left(1 - \frac{d_i}{\rho_i}\right) \quad i,j=1,2; i \neq j \quad (13.56)$$

$$\text{Equivalent length} \quad : \quad L^* = d_1 + d_2 - Dd_1d_2 \quad (13.57)$$

$$\text{Equivalent } G\text{-parameter} \quad : \quad G^* = 2g_1^*g_2^* - 1 \quad (13.58)$$

$$\text{Magnification (round trip)} \quad : \quad M_1^* = G^* \pm \sqrt{G^{*2} - 1} \quad (13.59)$$

$$\text{Magnification (transit)} \quad : \quad M_2^* = g_1^* \pm \sqrt{G^{*2} - 1} / (2g_2^*) \quad (13.60)$$

$$\text{Equivalent Fresnel number} \quad : \quad N_{eq}^* = a^2 \sqrt{G^{*2} - 1} / (2L^*g_2^*\lambda) \quad (13.61)$$

$$\text{Wavefront curvature} \quad : \quad R_t^* = \frac{L^*}{L^*/\rho_1 - g_1^* + M_2^*} \quad (13.62)$$

In (13.59) and (13.60), the positive sign applies to positive branch, the negative sign to negative branch unstable resonators. In order to operate an unstable lens resonator efficiently over a wide refractive power range, it is necessary to minimize the sensitivity of the magnification and the wavefront curvature to the refractive power of the thermal lens. There are three basic resonator schemes to choose from, operating in different quadrants of the stability diagram. Although their sensitivity to the thermal lens is different, all three resonator schemes have in common that the optimum output coupling can only be attained at one fixed refractive power. An optimized unstable resonator design will provide maximum efficiency only at this point. For a positive branch unstable resonator, the resonator should be confocal at the design refractive power.

### 13.3.2 Positive Branch Confocal Unstable Resonators

We will now derive the design equation for a positive branch unstable lens resonator that becomes confocal at a certain refractive power  $D_0$  and provides maximum extraction efficiency at this point. As depicted in Fig. 13.38, both the magnification  $M_1^*$  and the equivalent Fresnel number  $N_{eq}^*$  of the lens resonator decrease as the refractive power is increased. When the resonator is confocal, both parameters should assume values  $M_0$  and  $N_{eq,0}$ , respectively, providing optimum output coupling. In addition, the active medium with radius  $b$  should be completely filled by the laser mode as shown in Fig. 13.35. This leads to four conditions:

$$M_1^*(D_0) = M_0 \tag{13.63}$$

$$N_{eq}^*(D_0) = N_{eq,0} \tag{13.64}$$

$$b = 1.05 M_0 a \tag{13.65}$$

$$M_2^* = g_1^* - L^*/\rho_1 \quad (\text{confocality}) \tag{13.66}$$

Since the unstable resonator has five parameters  $(a, d_1, d_2, \rho_1, \rho_2)$ , the resonator design is not completely defined by the four constraints (13.63)–(13.66). However, in general the distance  $d_2$  should be chosen as small as possible to minimize the influence of the amplifier region on the extraction efficiency. Therefore, it makes sense to express the resonator parameters as a function of  $d_2$ .

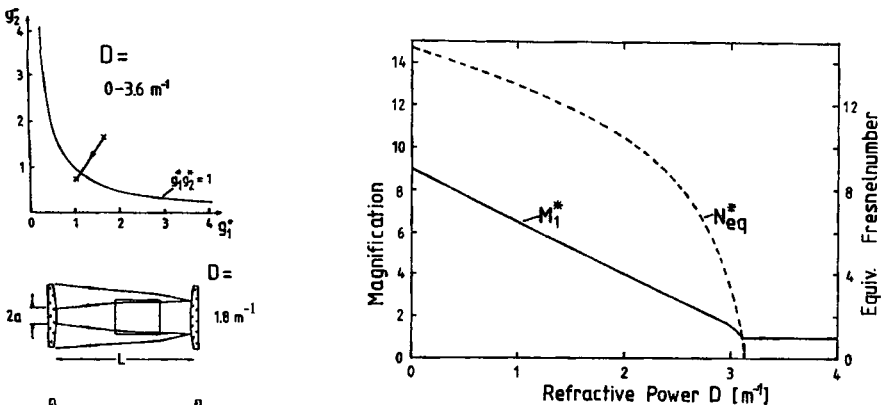
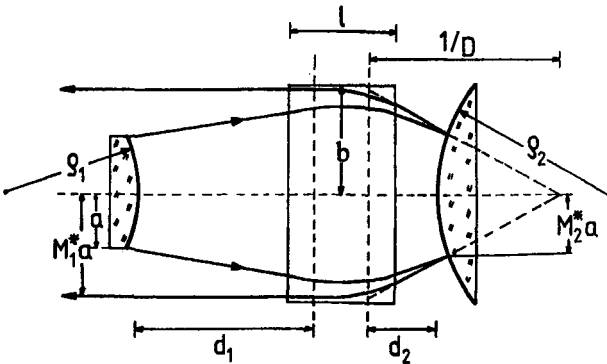


Fig. 13.38 Magnification and equivalent Fresnel number as a function of the refractive power for a positive branch unstable resonator ( $\rho_1 = -0.5 \text{ m}$ ,  $\rho_2 = -0.3 \text{ m}$ ,  $d_1 = 21 \text{ cm}$ ,  $d_2 = 13 \text{ cm}$ ). The left graphs show the equivalent g-diagram and the beam propagation for different refractive powers. The resonator is confocal at  $2.7 \text{ m}^{-1}$ .



**Fig. 13.39** The positive branch unstable resonator with an internal lens operating at the confocal point. The medium is filled by the beam, and the near field exhibits a flat phase distribution.

By using (13.60) and (13.61) in combination with the four constraints, the following system of design equations can be derived [4.104]:

$$a = \frac{b}{1.05 M_0} \tag{13.67}$$

$$\rho_1 = - \frac{b^2}{\lambda N_{eq,0} (1.05 M_0)^2} \tag{13.68}$$

$$d_1 = \frac{d_2 [2 - D_0 (M_0 - 1) \rho_1] + (M_0 - 1) \rho_1}{2 (D_0 d_2 - 1)} \tag{13.69}$$

$$\rho_2 = \frac{L^{*2}}{L^* (1 - D_0 d_1) - \frac{a^2 (M_0^2 - 1)}{4 M_0 N_{eq,0} \lambda}} \tag{13.70}$$

The combination of these four equations provides the resonator parameters for optimum performance at a refractive power  $D_0$ . The distance  $d_2$  is a free parameter. Note that the solution of (13.68) has to be inserted into (13.69) to get the distance  $d_1$ , and  $d_1$  serves as an input parameter for (13.70). For high power solid state lasers, the optimum magnification is around  $M_0=2$  and, for better transverse mode discrimination, the equivalent Fresnel number should be a half integer value. Figure 13.40 presents the solutions of (13.67)-(13.70) for this case as a function of the design refractive power  $D_0$ . For these graphs, a distance  $d_2$  between the principal plane of the lens and the unconfined mirror of 10cm was used.

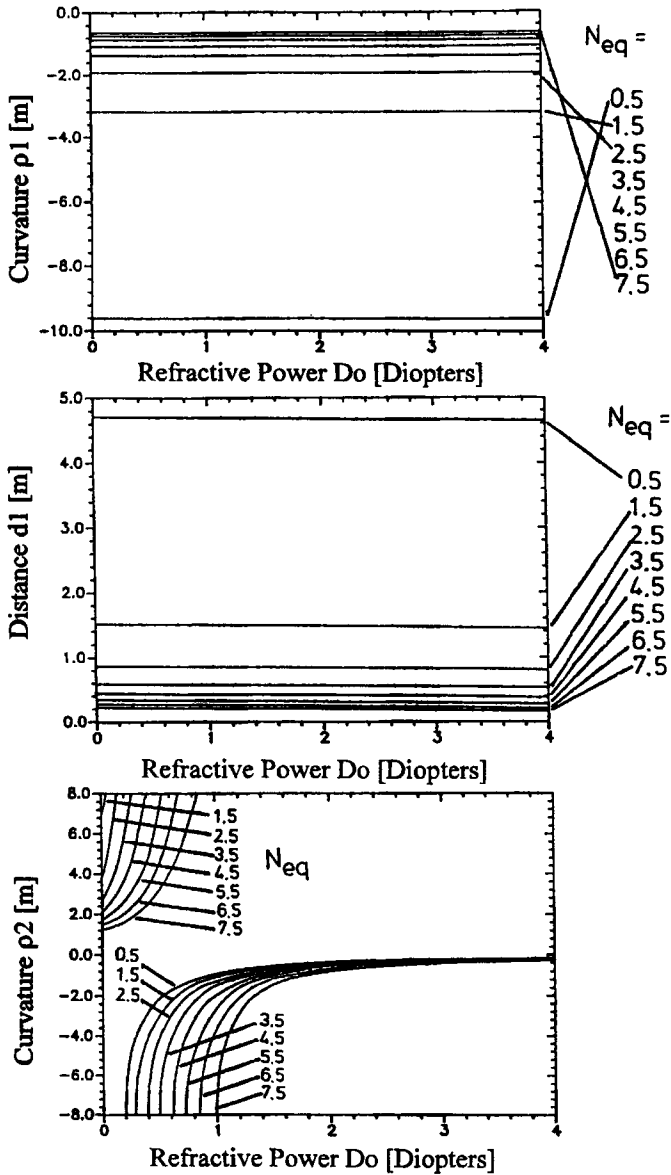


**Fig. 13.40** Optimum distance  $d_1$  and optimum mirror curvatures  $\rho_1, \rho_2$  as a function of the design refractive power  $D_0$  for positive branch unstable lens resonators in the first quadrant of the  $g$ -diagram. The lens resonator is confocal at the refractive power  $D_0$  with a magnification of  $M_0=2.0$  and an equivalent Fresnel number  $N_{eq,0}$  ( $b=5\text{mm}$ ,  $d_2=10\text{cm}$ ,  $\lambda=1.064\mu\text{m}$ ). The curve parameter is the equivalent Fresnel number  $N_{eq,0}$ .

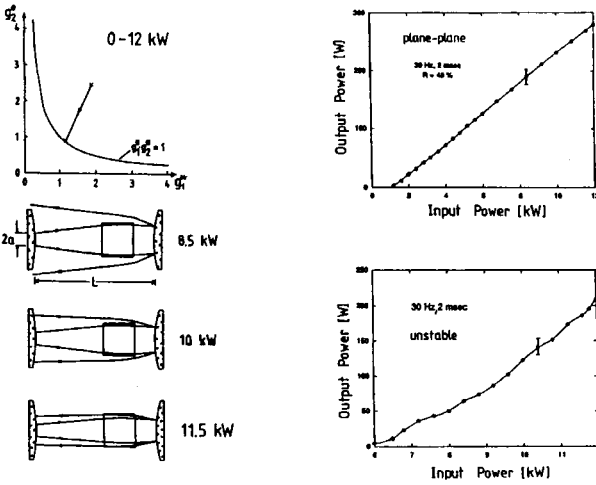


**Fig. 13.41** Measured output power for a pulsed Nd:YAG rod laser ( $b=5\text{mm}$ ,  $\ell=150\text{mm}$ ) with a positive branch unstable resonator (lower right graph). The refractive power of the rod is  $0.3\text{m}^{-1}$  per kW of input power. The left graph depicts the equivalent g-diagram and the beam propagation for different input powers. The resonator is confocal with a magnification  $M_0=2$  at an input power of  $11.5\text{kW}$  ( $\rho_1=-0.5\text{m}$ ,  $\rho_2=-0.3\text{m}$ ,  $d_1=27\text{cm}$ ,  $d_2=12\text{cm}$ ,  $a=2.0\text{mm}$ ). The upper right graph shows the output power measured with a symmetric flat-flat resonator (geometrical length:  $1.15\text{m}$ ) for comparison (pulse duration:  $2\text{ms}$ , repetition rate:  $30\text{Hz}$ , maximum pump energy:  $720\text{J}$ ) [4.104] (© Chapman & Hall 1990).

The experimental data presented in Fig. 13.41 indicate that the positive branch unstable resonator exhibits a high laser threshold. This is due to the high initial magnification of  $M_I=14$  that is required to keep the resonator in the unstable zone over the whole pump power range. For lasers that comprise a strong thermal lens, this resonator exhibits a very limited operating range around the confocal point since both the magnification and the wavefront curvature at the output coupler depend strongly on the refractive power. Furthermore, the confocal resonators are very close to the stability limit. A slight increase of the pump power will thus drive the resonator into the stable zone. If a high reflecting output coupler is used, accidental penetration into the stable zone may damage the mirror due to the high intracavity intensity (there is basically no output coupling in the stable zone). Therefore, it is advantageous to use a variable reflectivity mirror with a lower center reflectivity.

Compared to a stable resonator, unstable resonators generally provide only 60-70% of the output power. As was discussed in Sec.11, this decrease is caused by a lower fill factor and diffraction losses generated by the active medium. The sensitivity of the resonator properties to thermal lensing can be decreased considerably by using resonators in other quadrants of the stability diagram. One resonator scheme is the rod-imaging resonator [4.105], a negative branch unstable resonator operating in the fourth quadrant (Fig. 13.42).

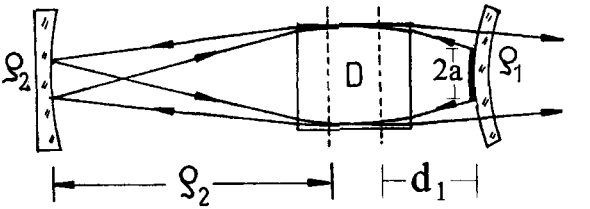


**Fig. 13.42** Beam propagation in a rod-imaging unstable resonator ( $\rho_1 = -0.3m$ ,  $\rho_2 = 0.4m$ ,  $d_1 = 13cm$ ,  $d_2 = \rho_2$ ,  $a = 3mm$ ,  $b = 5mm$ ). Mirror 2 images the left principal plane onto itself. The refractive power is  $D = 4.6m^{-1}$  [4.130] (© OSA 1993).

### 12.3.3 Rod-Imaging Unstable Resonators

Negative branch unstable resonators exhibit a much lower sensitivity of the magnification to thermal lensing compared with positive branch resonators. This low sensitivity stems from the positive radius of curvature of one mirror which also produces a focal point inside the cavity. A careful resonator design, however, is required because the focal point must not be located too close to the active medium. A useful design is the rod-imaging resonator [4.105,4.130], as shown in Fig. 13.42. The rear mirror 2 images the principal plane of the lens onto itself which means that the  $g$ -parameter of this mirror is constant:

$$g_2^* = g_2 - Dd_1 \left( 1 - \frac{\rho_2}{\rho_1} \right) = g_2 = -\frac{d_1}{\rho_2} \tag{13.71}$$

and the  $g$ -parameter of the output coupling mirror reads:

$$g_1^* = 1 - \frac{d_1 + \rho_2}{\rho_1} - D\rho_2 \left( 1 - \frac{d_1}{\rho_1} \right) \tag{13.72}$$

The resonator will thus move parallel to the  $g_1$ -axis in the equivalent  $g$ -diagram. Rod-imaging resonators are confocal if the condition:

$$g_1^* + g_2 = 2g_1^*g_2 \tag{13.73}$$

is met. Note that for rod-imaging resonators, both the magnification  $M_f^*$  and the equivalent Fresnel number  $N_{eq}^*$  are negative. Besides the lower sensitivity of the magnification (Fig.13.43), other advantages of rod-imaging resonators are the efficient filling of the active medium and a low misalignment sensitivity of the output coupling mirror.

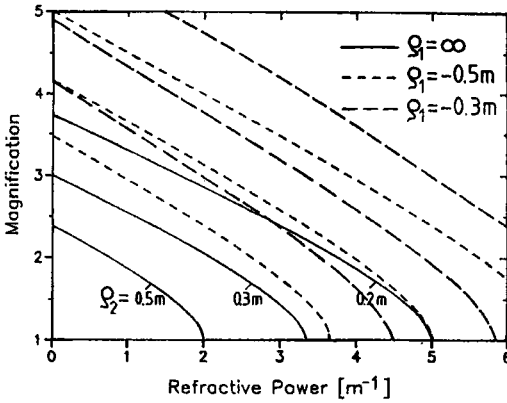


**Fig. 13.43** Dependence of the absolute value of the magnification  $M_1^*$  of rod-imaging unstable resonators ( $d_2 = \rho_2$ ) on the refractive power  $D$  for three different mirror curvatures  $\rho_1$ . The distance  $d_1$  is always 10cm; curves with the same line type differ in the mirror curvature  $\rho_2$  (higher magnification for smaller curvature) [4.130] (© OSA 1993).

Similar to the positive branch resonators, we can determine an optimized resonator design that provides a certain magnification  $M_0$ , a certain equivalent Fresnel number  $N_{eq,0}$ , and a collimated output beam at a refractive power  $D_0$  by applying the conditions (13.64)-(13.70). Since we have four resonator parameters ( $\rho_1, \rho_2, d_1, a$ ), there is only one resonator that can meet all four constraints. In order to have more freedom in the resonator design, let us drop the condition on the Fresnel number and express the curvatures as a function of the distance  $d_1$ . The following design equations hold for rod-imaging resonators that become confocal at the refractive power  $D_0$  with a magnification of  $M_0$  ( $b$ : radius of active medium):

$$a = \frac{-b}{1.05 M_0} \tag{13.74}$$

$$\rho_1 = d_1 \left[ D_0 + \frac{M_0 - 1}{2d_1} \right] / \left[ D_0 + \frac{M_0^2 - 1}{4M_0 d_1} \right] \tag{13.75}$$

$$\rho_2 = d_1 \frac{-2}{M_0 + 1} \tag{13.76}$$

Keep in mind that the magnification  $M_0$  is negative in these equations. The refractive power at which the resonator goes confocal is mainly controlled by the radius of curvature  $\rho_1$  of the output coupler. Figure 13.44 presents the radius of curvature  $\rho_1$  as a function of the design refractive power for different magnifications and different distances  $d_1$ .

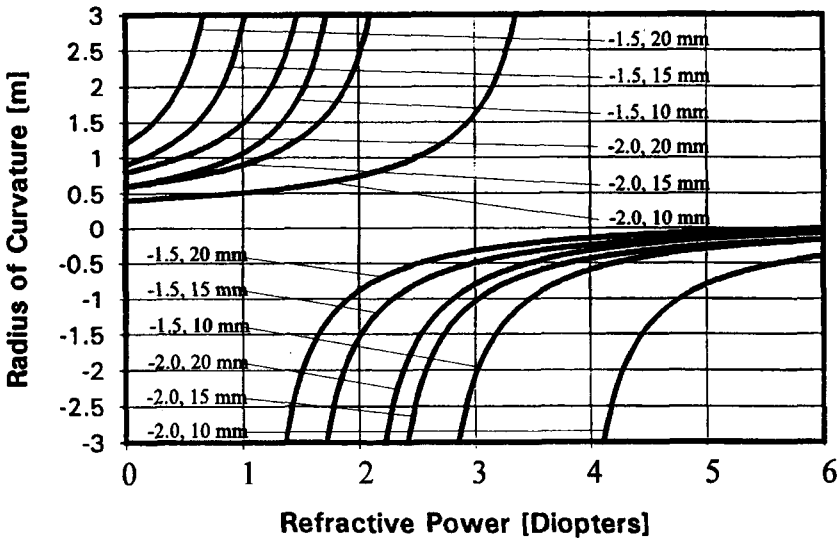


**Fig. 13.44** Radius of curvature of the output coupling mirror as a function of the refractive power  $D_0$  for rod-imaging unstable resonators that become confocal at the refractive power  $D_0$  with a magnification of  $M_0$ . The curve parameters are the magnification  $M_0$  and the distance  $d_1$ .

For high power Nd:YAG lasers that require a magnification of  $M_0=2$  at refractive powers around  $4\text{m}^{-1}$ , for instance, mirror radii of  $\rho_2=0.3\text{m}$  and  $\rho_1=-0.5\text{m}$  seem to be a reasonable choice if a distance of  $d_1=15\text{cm}$  is used. An experimental result for a pulsed Nd:YAG laser utilizing a similar resonator design is presented in Fig. 13.45. The resonator provides a magnification of 2.6 at the maximum refractive power of  $3.8\text{m}^{-1}$ . As we can see in the equivalent  $g$ -diagram, the rod-imaging condition is not exactly met (the  $g$ -parameter  $g_1$  increases slightly since  $d_1$  is 2mm too long). However, this slight mismatch, which is within the typical experimental tolerance, does not have a serious impact on the resonator performance. Since rod-imaging resonators can start at a lower magnification without being driven out of the unstable zone, the laser threshold is considerably lower as compared to confocal positive branch resonators. Again, the output power attained is lower compared to a stable resonator which for this laser head provided 520W at the maximum pump power.

It should be added that the rod-imaging unstable resonator does not necessarily have to be operated in a confocal point. It is true that the confocal resonator provides the highest fill factor, but the increase in extraction efficiency is almost negligible compared to non-confocal configurations. As far as the flat wavefront of the outcoupled beam is concerned, that can be realized in any resonator by using transformation optics right behind the output coupler. The design equations (13.74)-(13.76) should be considered as a suggestion. Any other resonator design that provides the right output coupling at the desired refractive power but is not confocal will probably perform as well.

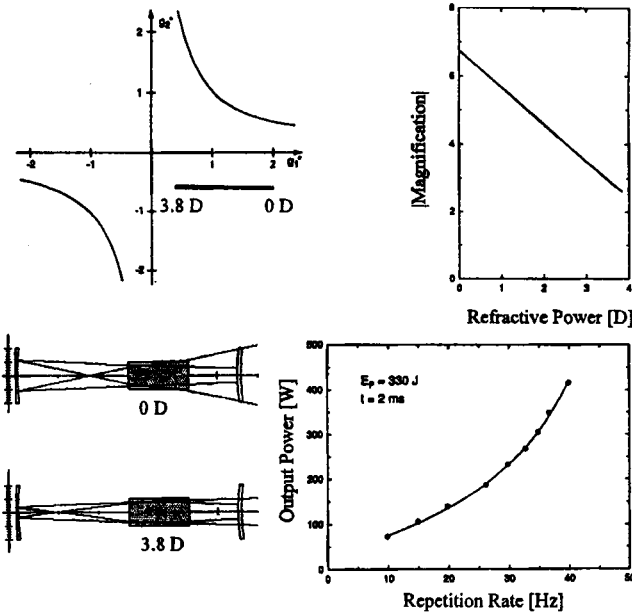


**Fig. 13.45** Measured output power of a pulsed Nd:YAG rod laser ( $b=5mm, \ell=150mm$ ) utilizing a rod-imaging resonator as a function of the repetition rate. The refractive power at 40Hz (electrical pump power of 13.2kW, pulse duration: 2 ms) is 3.8 Diopters. Resonator data:  $\rho_1=-0.5m, \rho_2=0.3m, d_1=16cm, d_2=32cm, a=2.5mm$ . The magnification as a function of the refractive power, the equivalent g-diagram, and the beam propagation for minimum and maximum refractive power are also shown.

### 13.3.4 Near Concentric Unstable Resonators

In the rod-imaging resonator one principal plane was imaged onto itself resulting in one constant g-parameter. If both principal planes are imaged by the mirrors ( $d_1=\rho_1$  and  $d_2=\rho_2$ ), both g-parameters become independent of the refractive power and the lens resonator remains concentric with  $g_1 * g_2 = 1$ . By increasing the distances  $d_1, d_2$  by small amounts  $\Delta_1, \Delta_2$ , respectively, the lens resonator is moved into the unstable zone (Fig. 13.46). In this case, the g-parameters are not constant anymore, but, due to the proximity to the concentric resonators, they show a very low sensitivity to the refractive power. This is the concept of the near-concentric unstable resonator (NCUR) [4.107]. One special configuration is the symmetric NCUR with  $\Delta_1=\Delta_2=\Delta$  and equal mirror curvatures  $\rho_1=\rho_2=\rho$ . In this case, the equivalent g-parameters read:

$$g_1^* = g_2^* = -1 - \frac{\Delta}{\rho} [2 - D(\rho + \Delta)] \tag{13.77}$$

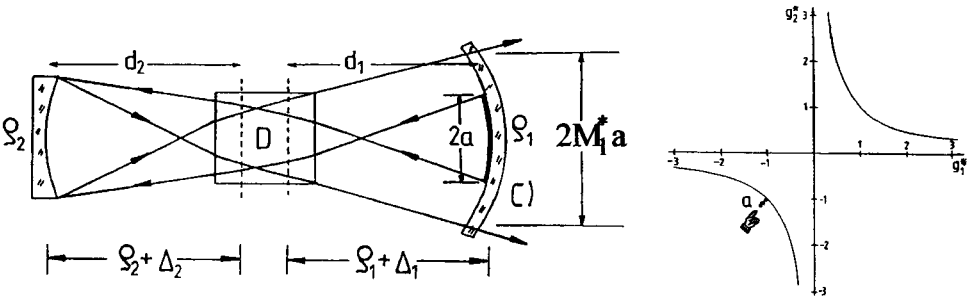


Fig. 13.46 The near concentric unstable resonator (NCUR) and its location in the  $g$ -diagram.

The refractive power  $D_{max}$  at which the resonator goes concentric again depends only slightly on the additional shift and is mainly determined by the mirror curvature. This refractive power also represents the range within which the NCUR can be operated:

$$D_{max} = \frac{2}{\rho + \Delta} \tag{13.78}$$

Therefore, it is possible to use this resonator for large ranges of refractive power by choosing the appropriate mirror curvature. The shift  $\Delta$  typically is on the order of 10-20mm. Figure 13.47 presents the magnification  $M_i^*$  as a function of the refractive power for different symmetric NCURs. Compared to the rod-imaging unstable resonator (see Fig. 13.43), the sensitivity of the magnification to thermal lensing is now further reduced. This is particularly true if small shifts  $\Delta$  and small mirror curvatures are used. However, small shifts  $\Delta$  are problematic since the two focal spots generated inside the resonator get too close to the active medium and may damage the endfaces. The shift  $\Delta$  should, therefore, never be smaller than 10mm if mirror curvatures between 0.3m and 0.5m are used. A lower sensitivity to the refractive power is also generated for the radius of curvature of the outcoupled wavefront, resulting in a smaller shift of the focus spot as the refractive power is increased (as we will see in the next section).

As far as the optimized resonator set-up (optimum magnification  $M_0$  at a refractive power  $D_0$ ) is concerned, the mirror curvatures and the shifts can be determined using a graph like the one in Fig. 13.47. The only parameter that needs a more careful treatment is the radius  $a$  of the output coupling mirror. Experimental results indicate that this radius has to be about 50% smaller than predicted by the geometrical beam propagation. If  $R_i^*$  denotes the radius of curvature of the wavefront (see Eq. (13.62)) at the refractive power  $D_0$  with magnification  $M_0$ , the radius  $a$  can, to a good approximation, be determined with:

$$a = 0.5 \frac{R_i^* b}{M_0 [R_i^* - \rho - \Delta + \ell/(2n)]} \tag{13.79}$$

where  $\ell$  is the length of the active medium,  $b$  is its radius, and  $n$  its refractive index.

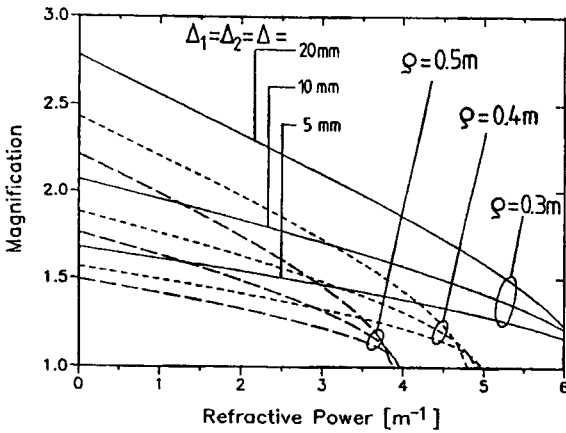


Fig. 13.47 Magnification  $M_i^*$  as a function of the refractive power for symmetric NCURs. The curve parameters are the mirror curvature  $\rho$  and the shift  $\Delta$  [4.107] (© OSA 1993).

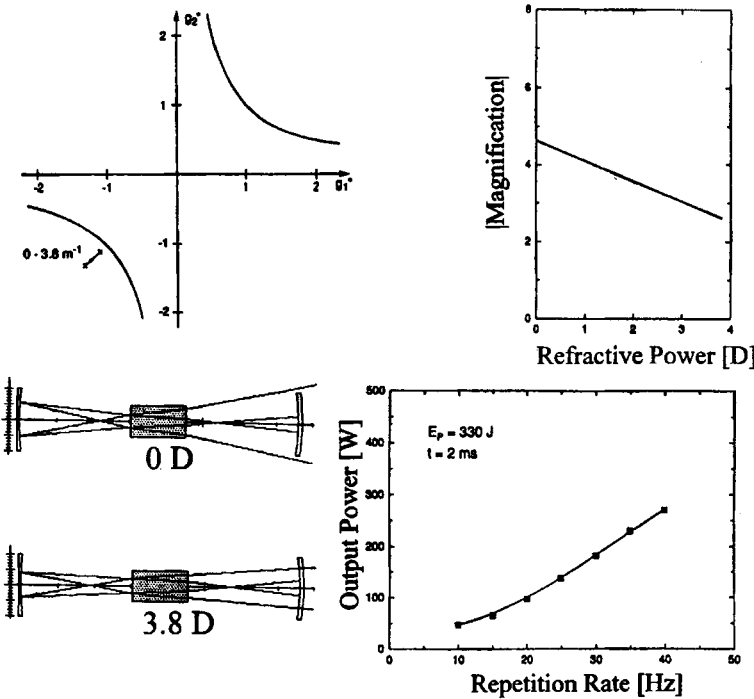


Fig. 13.48 Measured output power of a pulsed Nd:YAG rod laser ( $b=5$ mm,  $l=150$ mm) utilizing a NCUR as a function of the repetition rate. The refractive power at 40Hz (electrical pump power of 13.2 kW, pulse duration: 2ms) is 3.8 Diopters. Resonator data:  $\rho_1=0.3$ m,  $\rho_2=0.3$ m,  $d_1=35$ cm,  $d_2=36$ cm,  $a=2.5$ mm. The magnification as a function of the refractive power, the equivalent g-diagram, and the beam propagation for minimum and maximum refractive power are also shown.

### 13.3.5 Beam Quality and Focusing

The beam quality of unstable resonators is strongly affected by the spherical aberration of the thermal lens and the stress-induced birefringence of the active medium. In contrast to the operation of lasers without a thermal lens, where beam propagation factors  $M^2$  between 3 and 6 can be attained, the utilization of unstable resonators in high power solid state lasers provides beam qualities that are one order of magnitude lower. Typically, the focus consists of a bright spot with a diameter that corresponds to a  $M^2$  value of 10-15 surrounded by a wide low-intensity pedestal that contains about 50% of the output power. If a CCD camera or any other detector with spatial resolution is used to determine the beam quality, this pedestal goes undetected due to a low signal-to-noise ratio (typically 100:1). Figure 13.49 shows measured output power and beam parameter products (determined with an 8 bit CCD-imaging system) for a pulsed Nd:YAG rod laser using three different unstable resonator schemes presented earlier. All three resonators provide the same maximum output power and similar beam parameter products. Although these beam parameter products seem very low compared to those of stable resonators in multimode operation (25mm mrad at 400W output power), the power content is only 50% since the low intensity pedestal cannot be resolved by the CCD camera. This is clearly demonstrated in Fig. 13.50 in which two CCD images of the focus spot are shown, one at the nominal intensity used for the measurement and one at a 100 times higher intensity to visualize the side lobes. The corresponding power-in-the-bucket measurement indicates that the center spot contains about 50% of the total power. In order to use the laser beam for any application the pedestal has to be cut off with a spatial filter.

At present, the physical mechanisms leading to the beam quality deterioration are not yet understood. There is evidence that the birefringence in combination with the spherical aberration of the lens has a negative impact on the beam quality [3.209]. On the other hand, similar problems have been reported for low power solid state lasers where thermal lensing should not have much effect on the resonator properties. However, the problem seems to be restricted to solid state lasers since high power gas lasers (in the 10kW range and higher) utilizing unstable resonators provide beam propagation factors in the expected range of  $M^2=3-6$ .

One other problem of unstable resonators with a thermal lens is the dependence of the near field phase curvature  $R_i^*$  (see Eq. 13.62) on the pump power. The curvature  $R_i^*$  will vary between a value  $R_1^*$  at the minimum pump power and a value  $R_2^*$  at the maximum pump power. If a focusing lens is placed right behind the output coupler, the distance  $x$  of the focus spot is given by (Fig. 13.51):

$$x = f \frac{1}{1 - f/R_i^*} \quad (13.80)$$

and the total shift  $\Delta x$  of the focal distance over the whole pump power range reads:

$$\Delta x = f^2 \left| \frac{R_2^* - R_1^*}{(R_2^* - f)(R_1^* - f)} \right| \quad (13.81)$$

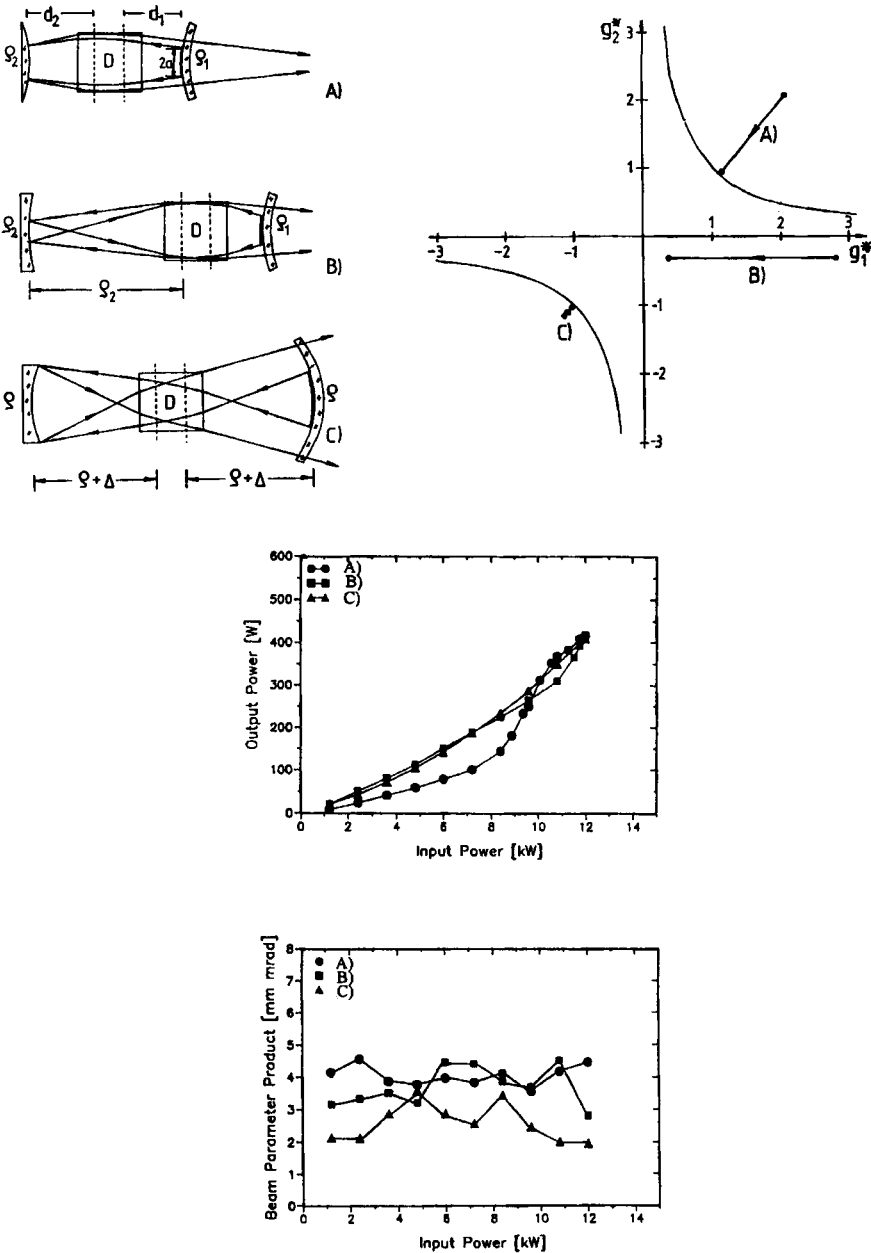


**Fig. 13.49** Measured output power and beam parameter products (50% power content) of a pulsed Nd:YAG laser ( $b=5\text{mm}$ ,  $l=150\text{mm}$ ) with three different unstable resonators. A) positive-branch confocal,  $\rho_1=-0.3\text{m}$ ,  $\rho_2=-0.3\text{m}$ ,  $d_1=15\text{cm}$ ,  $d_2=16\text{cm}$ ,  $a=2.5\text{mm}$ , B) rod imaging,  $\rho_1=-0.3\text{m}$ ,  $\rho_2=0.4\text{m}$ ,  $d_1=13\text{cm}$ ,  $d_2=40\text{cm}$ ,  $a=3\text{mm}$ , C) near concentric,  $\rho_1=0.3\text{m}$ ,  $\rho_2=0.3\text{m}$ ,  $d_1=32\text{cm}$ ,  $d_2=32\text{cm}$ ,  $a=4.5\text{mm}$ . The refractive power of the rod is  $0.38\text{m}^{-1}$  per kW of pump power (pulse duration: 2ms, pump energy: 240J). The beam propagation inside the resonators at the maximum refractive power of  $4.6\text{m}^{-1}$  and the paths in the equivalent  $g$ -diagram are shown in the upper graphs[4.130] (© OSA 1993).

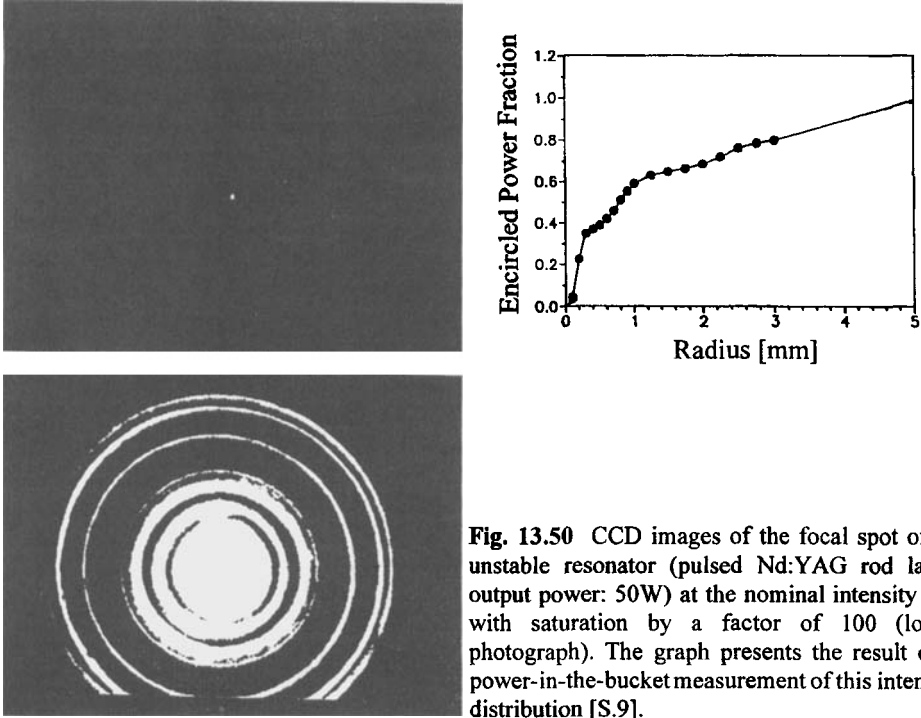


**Fig. 13.50** CCD images of the focal spot of an unstable resonator (pulsed Nd:YAG rod laser, output power: 50W) at the nominal intensity and with saturation by a factor of 100 (lower photograph). The graph presents the result of a power-in-the-bucket measurement of this intensity distribution [S.9].

Since the curvatures  $R_i^*$  are in general much larger than the focal length  $f$  we can approximate this expression by:

$$\Delta x = f^2 \left| \frac{R_2^* - R_1^*}{R_1^* R_2^*} \right| = f^2 \left| \frac{1}{R_1^*} - \frac{1}{R_2^*} \right| = f^2 S \quad (13.82)$$

The shift sensitivity  $S$  is equal to the variation of dioptric power of the output beam. In order to get a small shift of the focus, a resonator set-up providing a low shift sensitivity  $S$  must be found. Unfortunately, the determination of the shift sensitivity is not sufficient to characterize the focusing performance of a resonator, since  $S$  can be arbitrarily changed by means of transformation optics. An increase of the beam radius will decrease the shift sensitivity. However, the product of the beam radius and the shift sensitivity is a constant of the resonator, which means the shift sensitivities of different resonators can be compared if they exhibit similar beam radii at the output coupler. Figure 13.51 presents average beam radii on the output coupling mirror versus the shift sensitivity  $S$  for various positive branch and negative branch unstable resonators. This graph was calculated using (13.82) and the relations (13.56)-(13.62) for a rod radius of  $b=5\text{mm}$  and a maximum refractive power of  $4.6\text{m}^{-1}$ . This figure clearly shows that the near concentric resonator (curve *a*) provides the best means to obtain good constancy of the focal distance. The experimental verification of this statement is presented in Fig. 13.52, in which the distance  $x$  of the focal spot for the three resonators of Fig. 13.49 is shown as a function of the pump power.

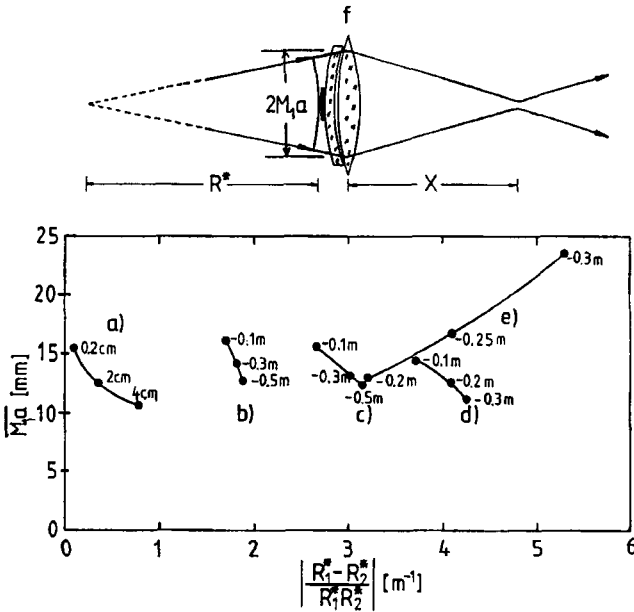


**Fig. 13.51** The radius of curvature  $R^*$  of the near field wavefront changes as the pump power is increased resulting in a variation of the focal distance  $x$ . The lower graph presents the average beam radius on the output coupler versus the shift sensitivity  $S$  (13.82) for different unstable resonators for a variation of the refractive power between 0 and  $4.6 \text{ m}^{-1}$  and a rod radius of 5mm. a) near concentric,  $\rho_1=0.3m, \rho_2=0.3m$ , parameter:  $\Delta$ ; b) rod imaging,  $\rho_2=0.2m, d_1=13cm$ , parameter:  $\rho_i$ ; c) rod-imaging,  $\rho_2=0.3m, d_1=13cm$ , parameter:  $\rho_i$ ; d) rod imaging,  $\rho_2=0.5m, d_1=13cm$ , parameter:  $\rho_i$ ; e) positive branch confocal,  $\rho_2=0.3m, d_1=15cm, d_2=16cm$ , parameter:  $\rho_i$  [4.130] (© OSA 1993).

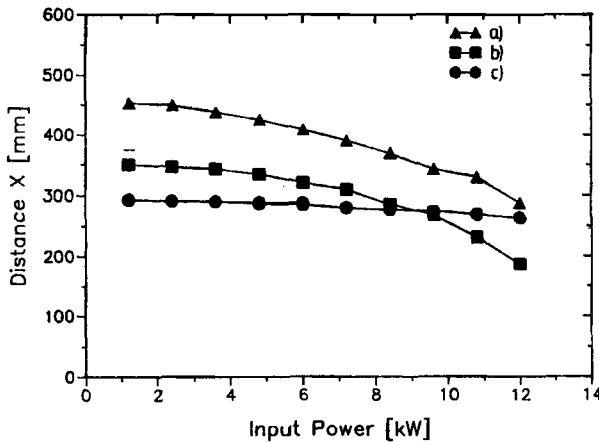


**Fig. 13.52** Measured distance  $x$  between the beam waist and the focusing lens as a function of the input power for the resonators presented in Fig. 13.46. The lens with focal length  $f=200mm$  was positioned 260mm behind the output coupler. a) positive branch confocal; b) rod-imaging, c) near concentric [4.130] (© OSA 1993).